

The Lyman alpha morphology of local starburst galaxies: release of calibrated images

Göran Östlin¹

Department of Astronomy, Stockholm University, AlbaNova University Center, 10691 Stockholm, Sweden
 ostlin@astro.su.se

Matthew Hayes

Geneva Observatory, University of Geneva, 51 chemin des Maillettes, 1290 Sauverny, Switzerland
 matthew.hayes@unige.ch

Daniel Kunth

Institut d'Astrophysique de Paris, Paris (IAP), 98 bis boulevard Arago, 75014 Paris, France

J. Miguel Mas-Hesse²

Centro de Astrobiología (CSIC-INTA), E28850 Torrejón de Ardoz, Madrid, Spain

Claus Leitherer

Space Telescope Science Institute, 3700 San Martin Drive, Baltimore, MD 21218, US

Artashes Petrosian

Byurakan Astrophysical Observatory and Isaac Newton Institute of Chile, Armenian Branch, Byurakan 378433, Armenia
 and

Hakim Atek

Institut d'Astrophysique de Paris, Paris (IAP), 98 bis boulevard Arago, 75014 Paris, France

ABSTRACT

We present reduced and calibrated high resolution Lyman-alpha ($\text{Ly}\alpha$) images for a sample of six local star forming galaxies. Targets were selected to represent a range in luminosity and metallicity and to include both known $\text{Ly}\alpha$ emitters and non-emitters. Far ultraviolet imaging was carried out with the Solar Blind Channel of the Advanced Camera for Surveys on Hubble Space Telescope in the F122M ($\text{Ly}\alpha$ on-line) and F140LP (continuum) filters. The resulting $\text{Ly}\alpha$

¹Oscar Klein Centre for Cosmoparticle physics, Department of Astronomy, Stockholm University, Sweden

²Laboratorio de Astrofísica Espacial y Física Fundamental (LAEFF-INTA), POB 78, Vva. Canada, Spain

images are the product of careful modeling of both the stellar and nebular continua, facilitated by supporting HST imaging at $\lambda \approx 2200, 3300, 4400, 5500, \text{H}\alpha$ and 8000\AA , combined with *Starburst 99* evolutionary synthesis models, and prescriptions for dust extinction on the continuum. In all, the resulting morphologies in $\text{Ly}\alpha$, $\text{H}\alpha$, and UV-continuum are qualitatively very different and we show that the bulk of $\text{Ly}\alpha$ emerges in a diffuse component resulting from resonant scattering events. $\text{Ly}\alpha$ escape fractions, computed from integrated $\text{H}\alpha$ luminosities and recombination theory, are found never to exceed 14%. Internal dust extinction is estimated in each pixel and used to correct $\text{Ly}\alpha$ fluxes. However, the extinction corrections are far too small (by factors from 2.6 to infinity) to reconcile the emerging global $\text{Ly}\alpha$ luminosities with standard recombination predictions. Surprisingly, when comparing the global equivalent widths of $\text{Ly}\alpha$ and $\text{H}\alpha$, the two quantities appear to be *anti-correlated*, which may be due to the evolution of mechanical feedback from the starburst. This calls for caution in the interpretation of $\text{Ly}\alpha$ observations in terms of star formation rates. The images presented have a physical resolution 3 orders of magnitude better than attainable at high redshifts from the ground with current instrumentation and our images may therefore serve as useful templates for comparing with observations and modeling of primeval galaxy formation. We therefore provide the reduced $\text{Ly}\alpha$, $\text{H}\alpha$, and continuum images to the community.

Subject headings: galaxies: ISM — galaxies: starburst — ultraviolet: galaxies — galaxies: individual (Haro 11, SBS 0335–052, IRAS 08339+6517, Tol 65, NGC 6090, Tololo 1924-416)

1. Introduction

The search for galaxies experiencing their first phase of violent star formation is one of the great challenges for observational cosmology. In this context, the importance of the Lyman-alpha emission line ($\text{Ly}\alpha$) can hardly be overstated. Young galaxies with low dust content should produce strong $\text{Ly}\alpha$ emission with equivalent widths, $W_{\text{Ly}\alpha}$, larger than 100\AA (Charlot & Fall 1993; Schaerer 2003). With a rest wavelength of 1216\AA the $\text{Ly}\alpha$ line is observable from the ground in the optical window at redshifts $z \sim 2$ to 6, and in principle in the near IR as far as $z \sim 20$.

Significant samples of galaxies can currently be established up to $z > 5$ using continuum (Lyman break, e.g. Iwata et al. 2003; Stanway et al. 2003; Bremer et al. 2004; Shimasaku et al. 2005) or emission line ($\text{Ly}\alpha$, e.g. Rhoads & Malhotra 2001; Hu et al. 2004; Venemans et al. 2004; Ouchi et al. 2005) techniques. However, while there is now much information regarding the continuum morphologies of galaxies and their evolution with redshift (e.g. Windhorst et al. 2002; Lotz et al. 2006; Ravindranath et al. 2006; Law et al. 2007), the situation is very different for $\text{Ly}\alpha$ where morphologies are all but unknown. At high- z ($\gtrsim 2$) when $\text{Ly}\alpha$ is observable from the ground, even the best seeing conditions result in observations with a spatial sampling of several kpc. At $z < 2$, space-based

observation becomes a requirement, although still very few instruments have been capable of emission line imaging in the UV. In the current study we take a first step towards remedying the almost complete lack of information regarding $\text{Ly}\alpha$ morphologies of local star forming galaxies.

First theoretical models proposed that primeval galaxies should be strong UV emitters both in continuum and line emission (Partridge & Peebles 1967; Meier 1976; Sunyaev et al. 1978), although early observations proved disappointing. However, at these times no high- z normal galaxies were known and the UV domain was terra incognita. An early attempt to study $\text{Ly}\alpha$ emission from three local star forming galaxies using the International Ultraviolet Explorer (IUE) found that $\text{Ly}\alpha$ emission was only present in the most metal-poor galaxy studied (Meier & Terlevich 1981). Subsequent studies of larger samples (Charlot & Fall 1993) confirmed a weak correlation of $\text{Ly}\alpha$ and the metallicity of the gas; not an unpredicted result given that the dust content generally correlates with metallicity. However, corrections for dust were found *not* to reconcile the $\text{Ly}\alpha/\text{H}\beta$ line ratios with those expected from recombination theory (Giavalisco et al. 1996) and it became clear from these early studies that some other processes must be at work. Indeed, resonant scattering of $\text{Ly}\alpha$ in HI had long been studied theoretically (Oster-

brock 1962; Adams 1972; Harrington 1974). The sub-recombination line ratios and low $W_{\text{Ly}\alpha}$ can be explained by multiple resonant scatterings locally trapping Ly α photons, redirecting them and causing them to traverse much greater integrated path lengths than non-resonant continuum or emission lines. Thus, even minute quantities of dust may result in significant or complete attenuation of Ly α (Neufeld 1990).

A major breakthrough in the detection of significant numbers of LAEs at high- z Ly α came with Cowie & Hu (1998), and today Ly α emission is arguably the most successful method for examining the galaxy population at the highest redshifts. Probing intrinsically fainter objects than the Lyman break technique, Ly α emission serves either as the spectral signature through which to identify high- z galaxy candidates or the definitive redshift identification of candidate objects. The impact on astrophysical cosmology has been enormous with Ly α surveys being used to study star-formation rates (Kudritzki et al. 2000; Fujita et al. 2003; Gronwall et al. 2007), large-scale structure (Venemans et al. 2004; Ouchi et al. 2005; Nilsson et al. 2007), test the ionization fraction of the intergalactic medium (Kashikawa et al. 2006; Dijkstra et al. 2007), and identify potential sites of population III star formation (Malhotra & Rhoads 2002; Shimasaku et al. 2006).

While it's difficult to argue against the impact of the high- z Ly α studies, some inconsistencies call for caution. Most notably that star-formation rates (SFR) in individual galaxies are often found to be lower when estimated by Ly α when compared with UV continuum (Ajiki et al. 2003; Taniguchi et al. 2005). Underestimates of the cosmic SFR density also tend to be underestimated by larger values when measured from LAEs (Rhoads et al. 2003; Kodaira et al. 2003). Moreover, LAEs have an inherent selection bias since only sources which show emission are included. In the sample of ~ 800 UV selected galaxies at $z \sim 3$, (also known as Lyman Break Galaxies (LBG) Shapley et al. 2003) found a median $W_{\text{Ly}\alpha}$ of $\sim 0\text{\AA}$, with only $\sim 25\%$ showing $W_{\text{Ly}\alpha} \geq 20\text{\AA}$. How these values evolve towards fainter continuum levels is unknown. Furthermore (Ouchi et al. 2003) noticed that bright LAEs appear more strongly biased against the underlying dark matter halo distribution than continuum-

bright sources. While the semi-analytical models for the space density of LAEs seem to be converging with the observed values (Le Delliou et al. 2005), uncertainties are still present and therefore open to discussion. In order to derive robust quantities from the LAE population, it is vital to understand the origin of these biases.

Again, results from low- z imply that the interpretation of Ly α observation at high- z may not be so clear-cut. High spectral resolution studies with HST showed the Ly α properties of local starbursts to be complex, in realizing that a low dust content is by no means a guarantee for observing Ly α in emission. Again, little correlation is found between Ly α emission or absorption and dust or metallicity (Kunth et al. 1994; Lequeux et al. 1995; Thuan & Izotov 1997). Kunth et al. (1998) clearly demonstrated that when Ly α is seen in emission it is systematically P Cygni in form and associated with signatures of an outflowing neutral ISM, while starbursts showing Ly α absorption features show no such outflow signatures. These results, also noticed at high- z in LBG spectra (e.g. Shapley et al. 2003), have profound implications for the escape of Ly α from starbursts: they suggest an outflowing medium to be a requirement in order for photons to avoid resonant trapping in the neutral medium. Hydrodynamic models (Tenorio-Tagle et al. 1999) predict an evolutionary sequence for the Ly α profile as a function of the mechanical energy return from the starburst, demonstrating how absorption, emission and P Cygni phases may all arise during different phases. Mas-Hesse et al. (2003) used this physical evolutionary scenario to interpret the range of Ly α profiles observed at low- z as an evolutionary sequence in the starburst population. To get a feeling for the astrophysics involved, we encourage the reader to look at Fig. 18 in Mas-Hesse et al. (2003).

Much theoretical effort has gone into the study of Ly α line profiles. Ahn (2004) and Verhamme et al. (2006) have examined the formation of P Cygni profiles from Lyman break-type galaxies, finding secondary emission peaks redwards of the P Cygni emission feature resulting from one or more backscatterings in the expanding neutral medium. Neufeld (1991) and Hansen & Oh (2006) have examined the transfer of Ly α in a multi-phase ISM. For models in which dust is embedded in dense H I clouds, they find that Ly α photons

can in fact preferentially avoid dusty regions and escape having experienced lower total dust optical depths than non-resonant photons. Thus equivalent widths may be artificially boosted, potentially causing ordinary star-forming objects to appear as more exotic systems.

What the low- z spectroscopic studies have not been able to accomplish is examination of global values relating to Ly α : spectroscopic observations miss the fraction (often the majority) of light which comes from outside the aperture or slit. This is highly likely to be the case for Ly α where resonant scattering may cause decoupling of Ly α from other wavelengths and Ly α photons may scatter in the galaxy and emerge far from their sites of production. Ionized holes or porosity in the ISM may also increase the chance of Ly α escape along certain paths. Ultimately, there is little evidence for the spatial correlation between Ly α emission and UV continuum at all. These considerations were the motivation for our pilot low- z imaging study of six local star-forming galaxies using the Advanced Camera for Surveys (ACS) on-board HST. The intent was to map Ly α morphology and study the effects of dust, kinematics, and luminosity on the escape of Ly α and the sample was hand-picked to reflect a range of these parameters. First results were presented in Kunth et al. (2003).

Besides Ly α , images have been acquired in H α and six continuum bandpasses between 1500Å and the I-band, enabling not only a comparison between Ly α and H α , but also detailed modeling of the stellar population and dust. Detailed studies have been presented for two galaxies in the sample, both low-metallicity UV-bright starbursts, ESO 338-04 and Haro 11 (Hayes et al. 2005, 2007). These studies found that emission and absorption varied on small scales in the central starburst regions, exhibiting very little correlation with the morphology probed by stellar continuum observations. Damped Ly α absorption was found in front of many UV-bright, young star clusters that must be a significant source of ionizing photons. Using H α , it was found that when Ly α does emerge from central regions, it is typically at surface brightness well below the value predicted by recombination theory. In contrast, large low surface brightness Ly α halos were found surrounding the central regions where typically Ly α /H α ratios and equivalent

widths exceed those predicted for recombination. Furthermore, modeling of the stellar population revealed that Ly α appears to emerge from regions either too old to produce ionizing photons and/or too dusty to permit the transfer of Ly α . Synthesis of these results points to the resonant scattering process being highly significant in the morphological structure.

It should be noted that these HST imaging observations are the only ones in existence that allow the comparison of Ly α with H α and stellar continuum and that they have a physical resolution, in the most distant case, 2 orders of magnitude better than that attainable at high- z under the best observing conditions. These data have now been fully processed, and continuum subtracted. Details of the continuum subtraction methodology can be found in Hayes et al. (2008), hereafter referred to as Paper I. In this article we discuss the Ly α line morphology, comparing it against H α and stellar continuum, and compute integrated fractions of escaping Ly α photons. The resolution of the data is so high that we believe them to be of interest for comparison with high- z samples of Ly α -emitting galaxies and also for the computational modeling of Ly α radiative transfer. As a service to the community we release the processed data on the *Centre de Données astronomiques de Strasbourg (CDS)*.

The article proceeds as follows: in Sections 2 and 3 we present the observations and data processing methods; in Section 4 we present the results, which we discuss in Section 5; Section 6 is dedicated to future perspective and possibilities; in Section 7 we present our concluding remarks and describe how to retrieve the released data.

Throughout this paper we will adopt $H_0 = 72 \text{ km s}^{-1} \text{ Mpc}^{-1}$ for the Hubble constant.

2. Observations

Six galaxies were selected for observations with HST. Since this is a pilot study, our sample is hand-picked. We aimed to provide a reasonable coverage of the starburst luminosity, metallicity and dust content. Four known Ly α emitters were included from the samples of Calzetti & Kinney (1992) and Kunth et al. (1998): Haro 11, IRAS 08339+6517, NGC 6090, and ESO 338-04; and two non-emitters from Thuan & Izotov (1997):

SBS 0335–052 and Tol 65. Since Ly α regulation is affected by ISM kinematics, selection of emitting targets was also based on the kinematic information imprinted on the observed spectroscopic line profile (Mas-Hesse et al. 2003). Our sample is summarized in Table 1.

The targets were observed with the Advanced Camera for Surveys (ACS) onboard the Hubble Space Telescope under two general observer programs: GO 9470 for acquisition of far UV data in the F122M and F140LP filters using the solar blind channel (SBC); and GO 10575 for obtaining H α , near-UV, and optical broad-band observations with the High Resolution (HRC) and Wide Field (WFC) cameras. The F122M observations were obtained during the ‘SHADOW’ part of the orbit in order to reduce the geocoronal Ly α background. In addition some complementary archival WFPC2 data was used. The observations are presented in Table 2.

3. Data reduction and processing

All¹ pipeline calibrated data from the different cameras were drizzled to the same scale (0.025"/pixel) and orientation using the task MULTIDRIZZLE in PYRAF. Remaining pixel shifts were fixed using the GEOMAP and GEOTRAN, and any remaining cosmic rays were removed using CREDIT. Next, all the images for a particular target were convolved to a common point spread function (PSF) using the image with the broadest PSF as a reference. This in general was F550M, except for SBS 0335–052 and Tol 65 where the archival I-band data had been obtained with the WF3 chip of WFPC2. Each image was then sky subtracted using FIT/FLAT_SKY in MIDAS using a low order (0 or 1) polynomial and a common sky region for the different passbands.

Obtaining Ly α line-only images has been shown to be a rather involved process, requiring the use of spectral model fitting, and is presented in Section 3.1. Model parameters selected for the fitting are discussed in Section 3.2. Fitting in turn requires a threshold signal-to-noise ratio to yield tolerable results, requiring binning of the data, discussed in Section 3.3.

¹With the exception of Tol 65 due to guide star problems, see Sect. 4.5

3.1. Continuum subtraction

Going from F122M and F140LP to continuum subtracted Ly α images is non-trivial for a number of reasons: the on-line filter is quite broad with a red wing, the effective wavelength of the off-line filter is rather far to the red side of the Ly α line, neutral hydrogen in the Milky Way absorbs part of the flux in the F122M filter, and the UV continuum is less well described by a power law near Ly α than at slightly longer wavelengths. In effect, adopting a simple assumption of a UV power-law ($f_\lambda \propto \lambda^\beta$) and neglecting the other effects mentioned can produce results ranging from strong Ly α emission to damped absorption simply by varying β . Indeed, Hayes & Östlin (2006) have shown that also for high- z imaging observations, estimation of the continuum at Ly α may be non trivial.

To overcome these limitations we have developed a method for continuum subtraction of ACS/SBC Ly α images. It is described in detail in (Hayes et al. 2008, hereafter Paper I) where we also perform thorough tests of the methodology and parameter dependencies. In short, the method utilizes *Starburst 99* (Leitherer et al. 1999, hereafter SB99) spectral evolutionary synthesis models and a set of UV and optical continuum band passes plus H α to perform a spectral energy distribution (SED) fit of up to two stellar and one nebular components, with reddening treated as a free parameter. The output is the *Continuum Throughput Normalization (CTN)* factor which determines how to scale the F140LP flux in order to accurately continuum subtract the F122M images.

The CTN is primarily dependent on the age and reddening of the stellar population dominating the UV flux. By sampling the UV spectral slope longwards of 1500Å and the 4000-break a non degenerate solution for CTN is obtained. Additional optical bandpasses and H α are included to constrain the contribution from an underlying older stellar population and ionized gas: Determining the continuum level at Ly α depends on fitting the stellar population age, which is sensitive to the strength of the 4000Å break. Contamination of this feature by an aged population that does not contribute to the continuum at 1216 Å could therefore result in erroneous age fits and estimates of CTN. Hence

Table 1: Target summary

Target name	Alternative name	RA(2000)	Dec(2000)	$E(B - V)_{\text{MW}}$	$\log(n_{\text{HI}})_{\text{MW}}$	v_r (km/s)	12+ $\log(\text{O}/\text{H})$	M_B	Em/Abs ^a	Ref
Haro 11	ESO 350-38	00:36:52.5	-33:33:19	0.049	20.4	6175	7.9	-20	Em	1
SBS 0335-052	SBS 0335-052E	03:37:44.0	-05:02:40	0.047	20.6	4043	7.3	-17	Abs	2
IRAS 08339+6517	PGC 024283	08:38:23.2	+65:07:15	0.092	20.6	5730	8.7	-21	Em	3
Tol 65	ESO 380-27	12:25:46.9	-36:14:01	0.074	20.7	2698	7.6	-15	Abs	4
NGC 6090	Mrk 496	16:11:40.7	+52:27:24	0.020	20.2	8785	8.8	-21	Em	3
ESO 338-04	Tol 1924-416	19:27:58.2	-41:34:32	0.087	20.7	2832	7.9	-19	Em	1

^aEm: known Ly α -emitter, Abs: known Ly α -absorber

NOTE.— $E(B - V)_{\text{MW}}$ is the Galactic extinction according to Schlegel et al. (1998) and $\log(n_{\text{HI}})_{\text{MW}}$ is the Galactic H I column density along the line of sight. Reference refers to nebular metallicity measurements: 1: Bergvall & Östlin (2002), 2: Papaderos et al. (2006), 3: Gonzalez Delgado et al. (1998), 4: Izotov et al. (2001)

the need for a two population SED fit. The philosophy is similar regarding the Balmer jump which may be significant where H II shells or filaments are well resolved, and is accounted for by treating nebular continuum independently.

The H α images have been continuum subtracted within the SED fitting software and have been corrected for the contribution from [N II] using literature data.

For all targets but two we have used two stellar plus one nebular component in the continuum subtraction (this is referred to as method v in Paper I). For IRAS 08339+6517 and Tol 65 we did not have sufficient data for this purpose and used an SED fit with fewer components (see Sect. 4.5).

3.2. *Starburst 99* and continuum modeling parameters

For this paper we use a standard setup of model parameters: A Salpeter (1955) IMF ($\alpha = 2.35$, $dN \propto M^{-\alpha} dM$) with lower and upper mass limits of 0.1 and 120 M_{\odot} , respectively. To model the starburst and underlying stellar populations we use instantaneous burst (single stellar populations); Geneva tracks with enhanced mass loss, and Pauldrach/Hillier atmospheres for the UV were used throughout. While derived ages and reddenings are more sensitive to assumed model parameters, the derived CTN and hence Ly α flux is indeed much less sensitive (see Hayes et al. 2005, 2008). In general, the most important concerns are the use of correct metallicity and extinction

law. For all galaxies we have adopted the SMC reddening law (Prévot et al. 1984) since the intense UV radiation field of these galaxies tends to destroy the graphite component of the dust, leading to smooth extinction laws without the 2175 Å feature, and thus providing consistently improved fits over other laws (e.g. Mas-Hesse & Kunth 1999). The effect of changing this is discussed in detail in Paper I.

For metallicity, we opt for the metallicity in *Starburst 99* closest to the observed nebular oxygen abundance (see Table 1). Hence for IRAS 08339+6517 and NGC 6090 we used $Z = 0.02$, for Haro 11 and ESO 338-04 we used $Z = 0.004$, and for SBS 0335-052 and Tol 65 we used $Z = 0.001$. Using Monte Carlo simulations (Paper I) we show that the accuracy of the continuum subtraction is not greatly affected, provided the assumed metallicity is within 50% of the true value. For all galaxies and metal abundances presented here, that is indeed the case.

3.3. Binning

For the continuum subtraction to yield photometrically reliable results a signal-to-noise (S/N) in each passband of between 5 and 10 is required (Hayes et al. 2008). This requires some smoothing or binning of the data in the low surface brightness regions. In order to simultaneously preserve the spatial information in the high S/N central regions, adaptive binning was used. We here make use of the Voronoi binning code of Diehl & Statler

Table 2: Observations: HST filter names, central wavelengths, and exposure times in seconds.

Target / Filter λ_{central} (Å)	F122M 1274	F140LP 1527	F220W 2257	F330W 3362	F435W 4312	F550M 5582	FR656N variable	F814W 8121
Haro 11	9095	2700	1513	800	680	471	680	100
SBS 0335–052	9000	2700	1660	800	680	430	680	4400 ^a
IRAS 08339+6517	9000	3000	1590	730	360 ^c	560 ^c	1024 ^c	–
Tol 65	9095	2700	1728	800	680	498	680 ^d	3400 ^e
NGC 6090	9095	3000	1683	800	680	645	680	100
ESO 338–04	9000	3000	1800 ^b	900 ^b	800 ^b	830	1214	520 ^b

^a Archival WFPC2/WF3/F791W image originally obtained in program 5408 (PI: Thuan)

^b Archival WFPC2/PC data (F218W, F336W, F439W & F814W) from program 6708 (PI: Östlin)

^c Data obtained with ACS/HRC

^d Data not useful

^e Archival WFPC2/WF3/F814W image originally obtained in program 6678 (PI: Thuan)

NOTE.—Unless noted otherwise the F220W, F330W, F814W were obtained with ACS/HRC; and F435W, F550M, FR656N with ACS/WFC

(2006) which is a generalization of the binning algorithm of Cappellari & Copin (2003). We use the F140LP image and its variance map to bin together pixels to conglomerate groups (known as ‘spaxels’) to improve S/N locally, while conserving surface brightness. Each spaxel accretes pixels until a S/N of 10 has been attained or until the maximum spaxel size of 1600 pixels ($1 \square''$) was reached. The same binning pattern was then applied to the other passbands.

3.4. Uncertainties

The accuracy of the continuum subtraction as a function of the input parameters is addressed in Hayes et al. (2008), where noise is added to idealized observations using Monte-Carlo simulations. In that article we consider only idealized, model data. These Monte Carlo simulations found the uncertainty (including the *statistical* uncertainty arising from noise in our fitting procedure, and *systematic* uncertainty accounting for our own estimation of model parameters) on the Ly α flux in a given spaxel to be a function of equivalent width. In general this has been shown to be below 30% for EW(Ly α)=10 Å and S/N=10 (the fiducial minimum value set by the binning, Section 3.3), with the error decreasing with increasing EW(Ly α) and S/N.

In this paper we have in addition performed Monte-Carlo simulations to assess the statistical

uncertainties on the real data: to each spaxel, random errors have been added in accordance with the photometric uncertainties for each passband. For each galaxy 100 Monte Carlo realizations were performed. Thus, the 8 individual science images for each object were regenerated 100 times with each spaxel randomly replaced by a Gaussian variate of the original, in accordance with its error. From these we created 100 new continuum subtracted images for each target, retaining all the important statistics of the spaxels in the final frame. We conclude that the statistical errors on the *integrated* Ly α properties in Table 4 are very small, ranging from 4% in the case of Tol 65 to 0.5% for ESO 338–04. The statistical S/N for each individual spaxel is of course smaller in general: the luminosity weighted averages range from $\langle S/N \rangle_L = 0.26$ for Tol 65 to 4.9 for Haro 11. Statistical uncertainties on H α properties are in general orders of magnitude smaller.

A larger source of uncertainty is likely to be errors that result from sky subtraction and flat fielding. The uncertainty of the sky level were, for each passband and galaxy, again fed into a Monte-Carlo simulation in a similar manner to that described above. A very conservative result is that flatfield and sky subtraction residuals can at most cause global errors on the 20% level. Since these kind of errors, when present, tend to have low spatial frequency they are likely to affect the global levels

rather than causing pixel-to-pixel variations.

In addition we have estimated the uncertainties by calculating the standard deviation of the background of the resulting Ly α level outside the galaxies, at a scale of $1 \square''$, i.e. the maximum spaxel size (see Table 4).

4. Results

Various analyses are performed on the processed images: direct photometric analysis and comparison with model-determined properties. We examine both small-scale, local relationships and global quantities, and our results are presented in a number of Figures and Tables. More detailed analysis for individual targets have either been presented previously (Hayes et al. 2005, 2007) or will be the scope of subsequent papers.

4.1. Morphologies

In Figs. 1 and 2 we show images of our targets in the F122M and F140LP filters, and continuum-subtracted Ly α and H α images. In this article we make use of adaptive smoothing (using FILTER/ADAPTIV in MIDAS) and adaptive binning (Diehl & Statler 2006) techniques, both of which are widely used in the X-ray community. Smoothing results in images that are more pleasing to the eye, although less photometrically secure. We here show Ly α images that have been obtained by continuum subtracting unbinned data, and an adaptively smoothed version of the same image. F140LP FUV contours are overlaid on the smoothed Ly α image to guide the eye. Binning, on the other hand, strictly conserves local surface brightness and has consequently been used for the photometric analysis (Sect. 4.3 – 4.4, and Tables 4 and 5).

In Fig. 3 we show RGB color composites for our six targets, with H α in red channel, F140LP in green, and adaptively smoothed Ly α in blue. The intensity scale is set to show detail and in general the H α and optical emission can be traced to much larger radii than here apparent. Both greyscale and false-color composite images show Ly α morphologies that are strikingly different from those in UV and H α . In all galaxies we see a mixture of both emission and absorption although Ly α appears not to emanate from regions of highest FUV surface brightness and instead seems to be most

frequently seen from regions fainter in the continuum.

4.2. Considerations for quantitative Ly α photometry

Absorption of the stellar continuum, both in the Milky Way and internally, present a couple of caveats against accurate photometric analysis of the continuum-subtracted Ly α maps. A review of these caveats is thus warranted.

Ultraviolet aperture spectroscopy of two of our targets (SBS 0335–052 and Tol 65) have revealed damped Ly α absorption (Thuan & Izotov 1997). This is confirmed by the Ly α continuum subtractions for both these objects. However, all observations in F122M are also subject to Galactic HI absorption and in cases where the redshift is small, internal and Milky Way features may be blended. While our continuum subtraction software does correct for the Galactic absorption, internal absorption features may be disguised if the features overlap. This is indeed the case for Tol 65 and, to a much lesser extent, SBS 0335–052. In effect this may lead us to overestimate the emerging Ly α flux.

In several cases when Ly α has been detected in high resolution spectroscopy it is found to have a P Cygni profile due to outflows in the neutral ISM that promote the escape of Ly α (Kunth et al. 1998). When the profile is unresolved, as is the case in low-resolution spectroscopy or narrow-band imaging, the absorption on the blue side may cancel part of the emission. It should be noted, however, that scattering alone does not lead to a reduction in flux, but rather a modified morphology and/or redistribution in frequency. Indeed, Verhamme et al. (2006) note that P Cygni profiles can arise as a natural consequence of radiation transfer in a moving medium, with no net loss of photons.

Whether moving neutral media will give rise to net emission or absorption not only depends on the HI density and outflow velocity but also on the relative contribution of the line and UV continuum, which of course are well resolved at low- z . If the continuum is strong, as in front of UV-bright star clusters, then any absorption could potentially be strong as well, increasing the likelihood of measuring net absorption. Indeed, in

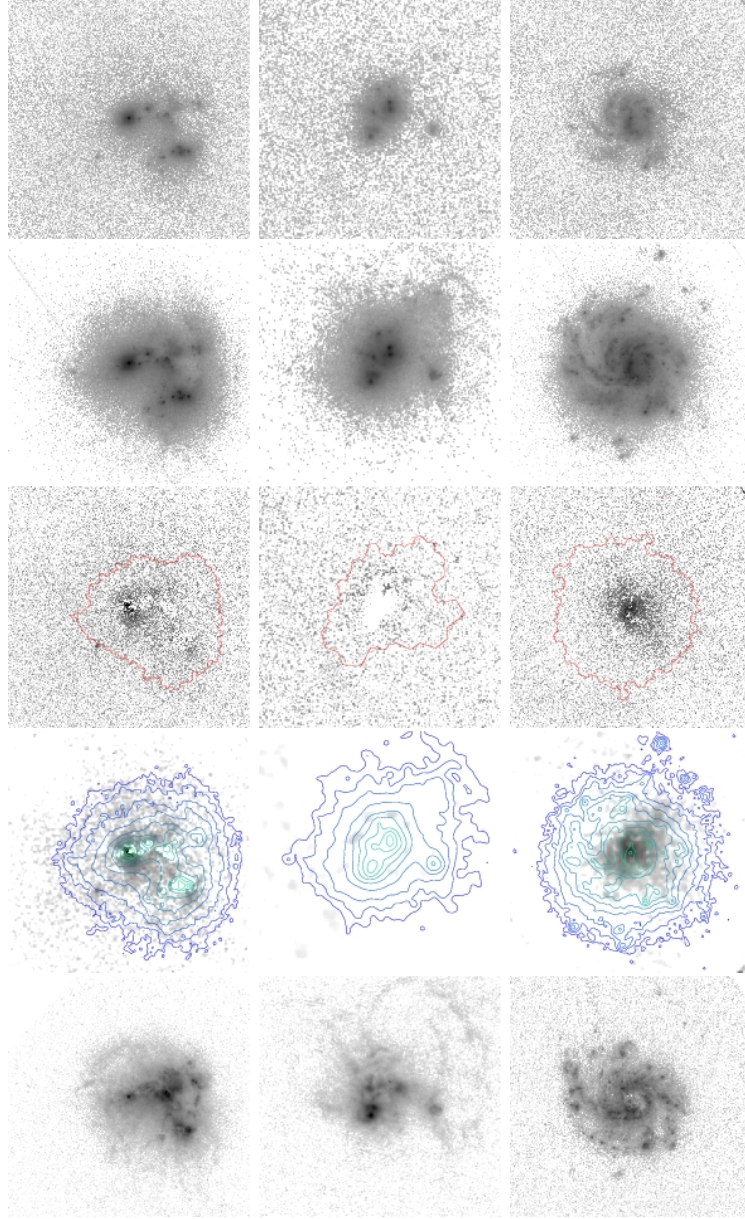


Fig. 1.— Greyscale images. From *top* to *bottom*: Reduced F122M and F140LP; continuum subtracted $\text{Ly}\alpha$ resulting from unbinned images but with the $\mu_{AB,1500} = 23 \text{ mag}/\square''$ isophotal mask generated from binned data overlaid; adaptively filtered $\text{Ly}\alpha$ with F140LP isophotes overlaid; and continuum subtracted unbinned $\text{H}\alpha$. The isophotal mask from the binned data is used later for quantitative photometry. The FUV contours show $25 \text{ mag}/\square''$ as the faintest isophote, with each subsequent isophote representing an increase by $1 \text{ mag}/\square''$. All intensity scaling is logarithmic. North is up, East to the left. Images are square cutouts with the length of one side in arcsec given in parentheses. From *left* to *right*: Haro 11 ($20''$), SBS 0335–052 ($10''$) and IRAS 08339+6517 ($20''$). In some images residual features from the ACS/SBC detector gap are visible. These areas have not been included in the photometry.

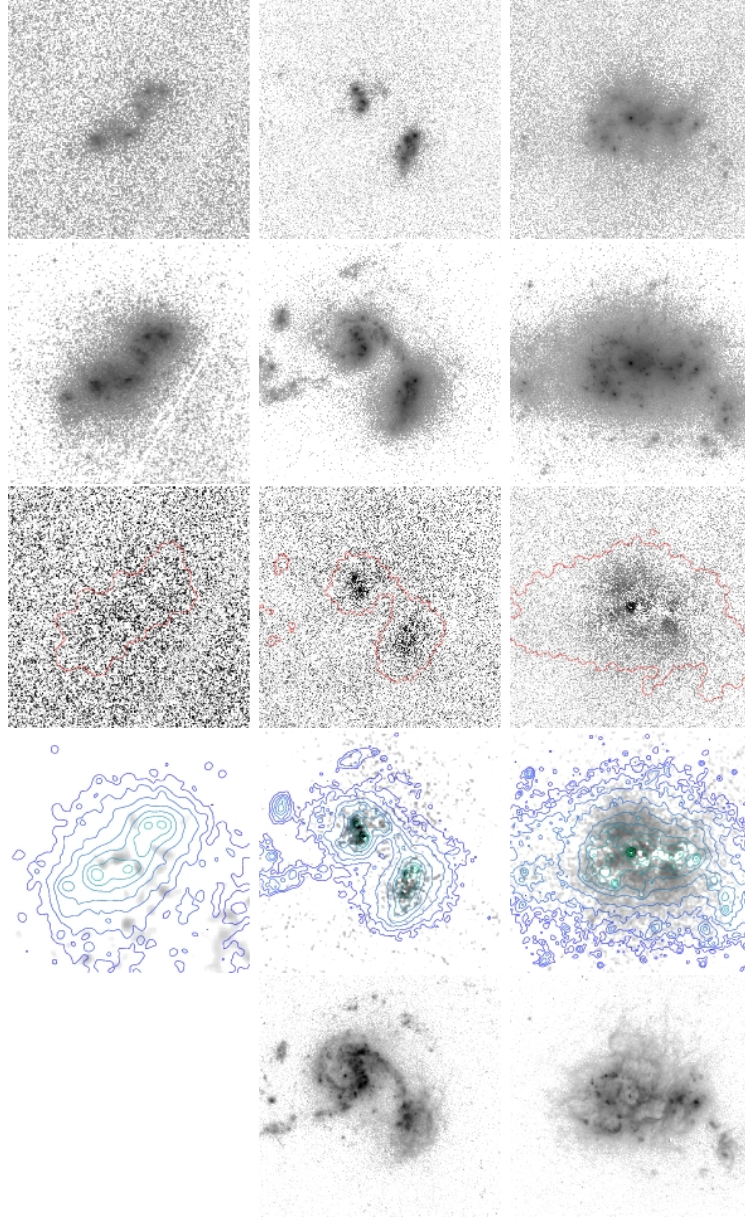


Fig. 2.— Greyscale images. As in Fig. 1. From *top* to *bottom*: F122M, F140LP, $\text{Ly}\alpha$, adaptively filtered $\text{Ly}\alpha$ with F140LP isophotes overlaid, and $\text{H}\alpha$. From *left* to *right*: (size in arcsec in parentheses): Tol 65 ($10''$), NGC 6090 ($20''$) and ESO 338-04 ($20''$). The intensity scaling is logarithmic. North is up, East to the left.

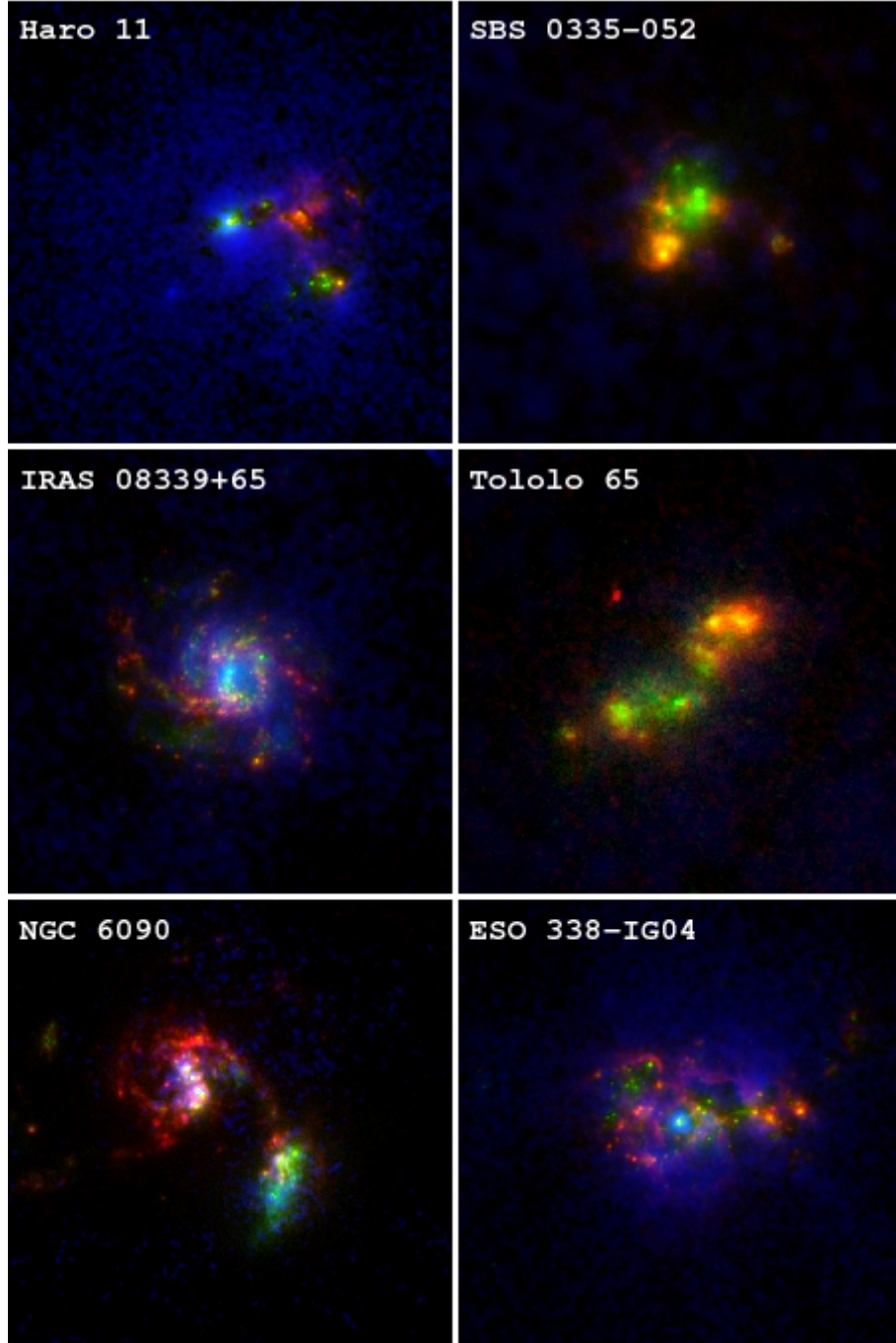


Fig. 3.— Color composite images of the whole sample. The blue channel shows continuum subtracted $\text{Ly}\alpha$, adaptively smoothed for the sake of presentation. Continuum subtracted $\text{H}\alpha$ is shown in red. 1500\AA continuum is shown in green. The intensity scaling is logarithmic and arbitrary and has been adjusted to show interesting details. Each image has a size of $15'' \times 15''$, except for SBS 0335-052 ($5'' \times 5''$) and Tol 65 ($7.5'' \times 7.5''$). For Tol 65 the red channel shows a mixture of $\text{H}\beta$, $[\text{OIII}]$ and $\text{H}\alpha$ (see text for details). East is left, North is up. Low surface brightness $\text{Ly}\alpha$ emission can clearly be seen surrounding compact UV point sources, particularly in ESO 338-04, Haro 11, and the South West knot of NGC 6090.

a few cases we find local minima in Ly α surface brightness in front of UV-bright clusters that results from just this effect. On the other hand, in faint regions there is not much continuum to absorb. While the absorption feature itself may be undetectable in this regime, the blue wing of the emission profile may still be absorbed. When dust, of unknown distribution is added, it is impossible to know whether the ‘absorbed’ photons from the blue wing in any given pixel are (i) absorbed locally, (ii) scattered and absorbed elsewhere, (iii) scattered and emitted elsewhere, or (iv) scattered and redistributed in frequency to the red wing and emitted locally. Note that these effects will also be significant in typical high- z observations where the processes governing Ly α emission must be the same. What the true Ly α flux really is in the case of P Cygni-blended absorption and emission is a matter of definition. Here we naturally define Ly α as the sum of emission and absorption.

4.3. Quantitative global photometry and properties

We have extracted ‘global’ broad-band and emission line fluxes using a mask which was made by cutting the Voronoi-binned F140LP image at a surface brightness of level of $\mu_{AB,1500} = 23$ mag/arcsec², corrected for Galactic foreground reddening. The global quantities presented in Tables 3 and 4 have been integrated over these apertures. Table 3 also presents integrated far UV ($\lambda = 1527\text{\AA}$) luminosities and UV continuum slopes (β), derived from the F140LP and F220W images. In deriving β we used the pivot wavelengths, given in Table 3, but the effective wavelengths of a filter will in turn depend on the spectral shape, i.e. β . Hence the β values presented are only approximate, although since they are not actually used in the analysis, this is good enough.

Table 4 presents the derived Ly α and H α quantities. Regarding Ly α , we firstly quote the measured continuum-subtracted flux, $f_{Ly\alpha}$, which is the sum of all pixels (positive and negative) within the aperture. In addition we quote the sum of only the positive pixels, $f_{Ly\alpha}^+$, thereby rejecting all pixels that represent absorption of the stellar continuum. Note that our ability to resolve emission and absorption on small scales depends on the distance to the target. The integrated Ly α flux within our

apertures is in five cases positive and one case negative. The Ly α /H α ratios are an order of magnitude lower than the recombination value of 8.7 (Case B, Brocklehurst 1971). This indicates significant attenuation of Ly α due to dust, possibly aided by radiative transfer effects from H I. The Ly α equivalent widths ($W_{Ly\alpha}$) range from -37 to $+39$ Å, i.e. significantly smaller than for the theoretical predictions for young starbursts. To first order equivalent widths should be unaffected by reddening if the line and continuum are equally attenuated. The H α equivalent widths ($W_{H\alpha}$) appear anti-correlated with $W_{Ly\alpha}$ if anything (see Fig 7). For pure recombination one would expect $W_{H\alpha}$ and $W_{Ly\alpha}$ to be positively correlated, so clearly other effects than ordinary dust reddening must be at work.

In Table 5 we present quantities directly related to the escaping fractions of Ly α and dust extinction, integrated over the whole region of the mask. Firstly we present the Ly α escape fraction which has been calculated from:

$$f_{esc,Ly\alpha} = \sum f_{Ly\alpha} / (8.7 \times \sum f_{H\alpha,C}) \quad (1)$$

where $f_{H\alpha,C}$ is the H α flux corrected for the internal reddening found in our SED fit. This reddening is actually that of the stellar continuum and may hence be an underestimate for the nebular gas (e.g. Calzetti et al. 2000), which may in turn cause us to overestimate $f_{esc,Ly\alpha}$. See Atek et al. (2008) for an analysis of the nebular gas extinction in these galaxies. We find that $f_{esc,Ly\alpha}$ varies between 0 (SBS 0335–052; actually absorption so the measured escape fraction is negative) and around 14% (IRAS 08339+6517 and ESO 338–04). $f_{esc,Ly\alpha}^+$ is also presented, where only positive Ly α pixels are included in the summation. Rejection of negative pixels results in little change in the Ly α escape fraction for the galaxies that show few or weak absorption centers, (e.g. IRAS 08339+6517), significantly increases it in some cases (e.g. Haro 11 and Tol 65), and changes its sign in the case of SBS 0335–052, for which the escaping fraction of detectable photons is around 2%. In no cases does $f_{esc,Ly\alpha}^+$ reach above 20%.

Since we have an estimate of the internal reddening, we deem it meaningful to also use this value to de-redden the Ly α fluxes. This makes it possible to compute dust-corrected Ly α /H α

Table 3: Integrated broad band fluxes and magnitudes.

Target	$r_{eq,1500}$ ($''$) (kpc)	$\lambda = 1527$ f_λ m_{AB}	2255 f_λ m_{AB}	3360 f_λ m_{AB}	4320 f_λ m_{AB}	5580 f_λ m_{AB}	8115 f_λ m_{AB}	$\log(L_{FUV})$	β
Haro 11	5.4 2.2	5.21E-14 14.9	2.16E-14 15.0	1.09E-14 14.9	8.65E-15 14.6	5.12E-15 14.6	3.17E-15 14.3	10.3	-2.25
SBS 0335-052	3.1 0.83	1.24E-14 16.4	4.38E-15 16.7	1.71E-15 16.9	9.71E-16 16.9	4.08E-16 17.3	1.95E-16 ^a 17.4	9.3	-2.66
IRAS 08339+6517	5.9 2.2	9.04E-14 14.3	3.83E-14 14.4	2.37E-14 14.0	2.50E-14 13.4	1.70E-14 13.3	—	10.4	-2.21
Tol 65	2.3 0.42	4.26E-15 17.6	1.91E-15 17.6	7.46E-16 17.8	4.65E-16 17.7	1.95E-16 18.1	9.30E-17 ^b 18.1	8.5	-2.05
NGC 6090	4.0 2.3	1.71E-14 16.1	9.86E-15 15.8	6.81E-15 15.4	6.84E-15 14.8	5.18E-15 14.6	3.60E-15 14.2	10.1	-1.41
ESO 338-04	7.6 1.4	1.11E-13 14.1	—	2.16E-14 14.1	1.81E-14 ^c 13.7	1.25E-14 13.6	5.76E-15 ^b 13.6	9.9	-2.07

^aWavelength 7880

^bWavelength 8012

^cWavelength 4310

NOTE.—Integrated broad band fluxes and magnitudes within the isophotal mask ($\mu_{1500,AB} = 23$ mag/arcsec²). The second column gives the equivalent radius ($r_{eq} = \sqrt{\text{Area}/\pi}$) within which the fluxes were integrated in units of arcseconds (first line) and kpc (second line). First line gives f_λ in cgs units (erg s⁻¹ cm⁻² Å⁻¹), second line gives magnitudes in the AB-system. $L_{FUV} = \lambda \times L_\lambda$ in units of $L_{\odot, \text{Bol}} = 3.8 \cdot 10^{33}$ erg/s, and $\lambda = 1527$ Å. The UV-continuum slope is derived from f_{1500} vs. f_{2200} except for ESO 338-04 where we used f_{3360} rather than the available F218W image which is not as deep and quite affected by CR-residuals. All quantities have been corrected for Galactic extinction using the Schlegel et al. (1998) prescription.

ratios and dust-corrected Ly α escape fractions. Of course, if standard recombination theory was directly applicable, the corrected Ly α /H α ratio should be 8.7 and the dust-corrected Ly α escape fractions should be unity. Instead, the extinction-corrected Ly α fluxes are well below standard recombination predictions with factors ranging from 2.6 to infinity. In Table 5 we present $\mathcal{R} = \sum f_{Ly\alpha, C} / (8.7 \times \sum f_{H\alpha, C})$, i.e. the ratio of the extinction-corrected Ly α /H α to the recombination value and equivalently refers to the extinction-corrected ‘escape fraction’

Comparing $f_{esc, Ly\alpha}$ with \mathcal{R} reveals that (for galaxies with net emission) the latter is a factor 2 to 5 larger than the former. ESO 338-04 shows a Ly α escape fraction of almost 40% after de-reddening, and IRAS 08339+6517 approaches 30%. The ratio of \mathcal{R} to $f_{esc, Ly\alpha}$ is not significantly different when regarding positive pixels only, and therefore not presented. The emerging picture is hence that simple reddening corrections can’t come close to explaining the found escape fractions, meaning that in addition to simple dust reddening, other effects, i.e. resonant scattering

and ISM kinematics, appear to dominate the Ly α transport.

Of course, these Ly α escape fractions would be even lower if we have underestimated the total ionizing continuum radiation, i.e. if the true reddening of H α photons is larger than found by our SED fitting which could happen if there were some very deeply embedded sources that are completely absorbed in the UV. In Atek et al. (2008) we use ground based H α and H β images to estimate the dust extinction and consistently find even smaller escape fractions.

4.4. Small scale photometry and properties

In Figures 4 and 5 we show the Ly α surface brightness vs. H α , UV continuum, and β . The Voronoi binned resolution elements used to measure surface brightness vary in size between individual pixels in the central regions and 1600 pixel (1 \square'') spaxels in the faintest regions. Here we do not mask out the fainter regions as described for the integrated photometric measurements. In-

Table 4: Measured emission line properties.

Target name	$f_{\text{Ly}\alpha}$	$W_{\text{Ly}\alpha}$	$L_{\text{Ly}\alpha}$	$\sigma_{\text{Ly}\alpha}$	$f_{\text{H}\alpha}$	$W_{\text{H}\alpha}$	$L_{\text{H}\alpha}$	$\text{Ly}\alpha/\text{H}\alpha$
Haro 11 + only	9.30E-13 4.32E-12	15.6 25.5	8.40E+41 3.90E+42	4.0E-15	2.48E-12	704	2.24E+42	0.374 0.625
SBS 0335-052 + only	-6.77E-13 2.97E-14	-36.8 1.62	-2.59E+41 1.12E+40	2.9E-15	3.61E-13	1434	1.38E+41	-1.76 0.078
IRAS 08339+6517 + only	3.05E-12 3.52E-12	39.2 40.7	2.37E+42 2.73E+42	3.4E-15	2.37E-12	199	1.84E+42	1.29 1.54
Tol 65 + only	8.48E-14 1.47E-13	17.5 15.5	2.82E+40 4.89E+40	2.3E-15	1.85E-13	1300	3.41E+40	0.458 0.794
NGC 6090 + only	4.20E-13 5.71E-13	28.3 38.2	7.80E+41 1.06E+42	1.7E-15	1.27E-12	315	2.36E+42	0.330 0.449
ESO 338-04 + only	3.68E-12 4.99E-12	28.1 38.0	6.89E+41 9.35E+41	3.7E-15	2.61E-12	570	4.89E+41	1.41 1.91

NOTE.—Integrated galaxy properties within the far UV isophotal mask ($\mu_{1500,AB} = 23 \text{ mag}/\square''^2$). $\sigma_{\text{Ly}\alpha}$ is the ‘spaxel-to-spaxel’ standard deviation of the $\text{Ly}\alpha$ background outside the photometric aperture and hence measures the fluctuations on a one arcsecond scale. Note that this does not entirely reflect the error from flatfielding and sky subtraction which is conservatively found to be smaller than 20%. All quantities have been corrected for Galactic extinction using the Schlegel et al. (1998) prescription. Fluxes and luminosities are in cgs units, and equivalent widths in Å. The $\text{H}\alpha$ luminosity and equivalent width of Tol 65 has been derived from ground based observations (see text). The second line for each galaxy gives the result when including pixels with positive $\text{Ly}\alpha$ flux only.

stead, for inclusion of a spaxel, the criterion of having reached $S/N \geq 3$ in the F140LP image must have been fulfilled. This allows us to probe the fainter surface brightness regions while maintaining data reliability. Resolution elements in which the desired threshold $S/N \geq 10$ (See Hayes et al. 2008) has been met are shown in black, whereas pixels with $3 \leq S/N < 10$ are shown in blue. Since the pixel distribution plots use bins of various sizes, they cannot be used to estimate how the values are globally distributed and instead, histograms are presented above and to the side of the scatter plots in order to give some feeling for this. Moreover, since the surface brightnesses are presented in log-space, only pixels showing emission are included. Dashed lines on the $\text{Ly}\alpha$ vs. $\text{H}\alpha$ plots show the recombination line ratio of $f_{\text{Ly}\alpha} = 8.7 \times f_{\text{H}\alpha}$ and also the case $f_{\text{Ly}\alpha} = f_{\text{H}\alpha}$. On the $\text{Ly}\alpha$ vs. FUV plot the lines represent constant equivalent width of 1, 10, and 100 Å. These scatter plots show a number of characteristic features which we now discuss. For illustration several features are labeled (a–f) in the text and in Figures 4 and 5.

$\text{Ly}\alpha$ vs. $\text{H}\alpha$: A general feature is a sharp boundary at maximum $\text{H}\alpha$ surface brightness, at which $\text{Ly}\alpha/\text{H}\alpha$ ranges from unity and downwards (a), except for SBS 0335-052 where $\text{Ly}\alpha/\text{H}\alpha$ reaches the recombination value. The large range of values (extending to negative values, but which are not shown in these log-plots) is either the result of dust reddening or resonant scattering decoupling the $\text{Ly}\alpha$ photons from $\text{H}\alpha$. Another general feature is a ceiling in $\text{Ly}\alpha$ surface brightness at $\sim 10^{-13} \text{ erg/s/cm}^2/\text{arcsec}^2$ (b). While Haro 11 and ESO 338-04 present similar features, we see, in addition, a population of $\text{Ly}\alpha$ -bright spaxels with $\text{Ly}\alpha/\text{H}\alpha$ at, or above, the recombination value (c). In all galaxies an upper envelope is seen near or slightly above the recombination ratio, but at fainter $\text{H}\alpha$ levels a tail with super-recombination values develops – an indication of resonant scattering.

$\text{Ly}\alpha$ vs. UV continuum: A rather sharp boundary is seen at UV-bright levels ($\sim 10^{-14}$ to $10^{-15} \text{ erg/s/cm}^2/\square''/\text{\AA}$), reminiscent of a starburst intensity limit (d). From the combined UV

Table 5: Derived and reddening corrected properties.

Target	$f_{esc, Ly\alpha}(+)$	\mathcal{R}	$SFR_{H\alpha}$	$\log(L_{FIR})$	$SFR_{H\alpha}/SFR_{FIR}$	$E(B - V)_*$	$\log(L_{FUV,C})$
Haro 11	0.037 (0.062)	0.17	17.2	11.1	1.3	0.067	10.6
SBS 0335-052	-0.203 (0.009)	-0.28	1.1	9.3	2	0.044	9.45
IRAS 08339+6517	0.140 (0.168)	0.28	14.1	11.0	0.9	0.034	10.6
Tol 65	0.053 (0.091)	0.16	0.26	8.3	5	0.11	8.94
NGC 6090	0.027 (0.037)	0.13	18.2	11.4	0.4	0.19	10.8
ESO 338-04	0.139 (0.189)	0.39	3.9	9.8	3.4	0.076	10.2

NOTE.— $f_{esc, Ly\alpha}$ is the Ly α escape fraction obtained by dividing the observed (Galactic extinction-corrected only) Ly α flux by the H α flux corrected for Galactic *and internal* reddening (as a measure of the total intrinsic Ly α production) and the theoretical line ratio. \mathcal{R} is the same quantity but using the Ly α flux corrected for internal extinction. $SFR_{H\alpha}$ is based on the observed H α flux in Table 4 (not corrected for internal reddening) and uses the calibration by Kennicutt (1998). $\log(L_{FIR})$ is based on the 1.7 times the luminosity at 60 μ m (Chapman et al. 2000) as detected by IRAS and listed by NED, except for SBS 0335-052 and Tol 65 which were not detected by IRAS and where we have instead used the Spitzer values reported by Engelbracht et al. (2008). The FIR SFR calibration in $SFR_{H\alpha}/SFR_{FIR}$ uses the calibration by Kennicutt (1998). $E(B - V)_*$ is the color excess found in the SED fit for the integrated fluxes within the same far UV isophote as above.

and Ly α peak towards fainter UV surface brightness levels we see an upper envelope, which starts at $W_{Ly\alpha} \sim 30\text{\AA}$ at the bright end and approaches 1000 \AA at fainter ($\sim 10^{-17}\text{erg/s/cm}^2/\text{\AA}$) levels where it forms a tail with $W_{Ly\alpha} > 1000\text{\AA}$ (e). Again Haro 11 and ESO 338-04 present extra high surface brightness features with average equivalent widths of about 30 \AA .

Hence, we see regions where line ratios and equivalent widths are significantly enhanced compared to what would be expected from recombination theory and standard spectral synthesis models. This may naturally be expected to some extent for Ly α *vs.* FUV since ionized regions may be spatially separated from the UV, but for Ly α *vs.* H α it must imply that some process, resonant scattering, is causing Ly α to be emitted from regions where H α is very faint indeed.

Ly α / H α *vs.* β : Pixel-to-pixel variations between the Ly α /H α ratio and β again show little correlation as if Ly α emission was independent of the local stellar reddening. A tail in the distribution is also seen in these figures up to $\beta > 0$ (f). These red UV slopes indicate that either the stellar population is too old to produce nebular emission, or the dust reddening is too great to permit the transmission of Ly α . Either way, Ly α is seen in emission from these regions, and a significant fraction of the pixels show ratios greater than that of

case B recombination.

UV surface brightness: In Fig. 6 we show the fraction of Ly α fluxes emitted (or absorbed) within the masked regions as a function of the UV surface brightness. This is done by summing the flux in the pixels of the line-only image that fall within the surface brightness bins in the FUV image, then normalizing by the integrated flux within the masked region. Thus we can quantitatively assess how Ly α emission/absorption correlate with UV surface brightness. The same is also presented for H α and UV continuum itself. In most cases H α is clearly seen to be offset from the UV continuum since, to some varying degree, the bright stellar sources and ionized nebulae can be resolved. While the bulk of the emitted Ly α flux also appears to emerge from regions of lower FUV surface brightness, the distribution is further offset from that of H α .

4.5. Comments on individual targets

Haro 11 This target is extensively discussed in Hayes et al. (2007), where we also discuss X-ray data, the escape of Ly α as a function of the age of the stellar population (field stars and stellar clusters) and nebular reddening (from ground based observations). Kunth et al. (1998) found an asymmetric Ly α line in emission with no sign of Ly α emission at restframe 1216 \AA , suggesting Ly α es-

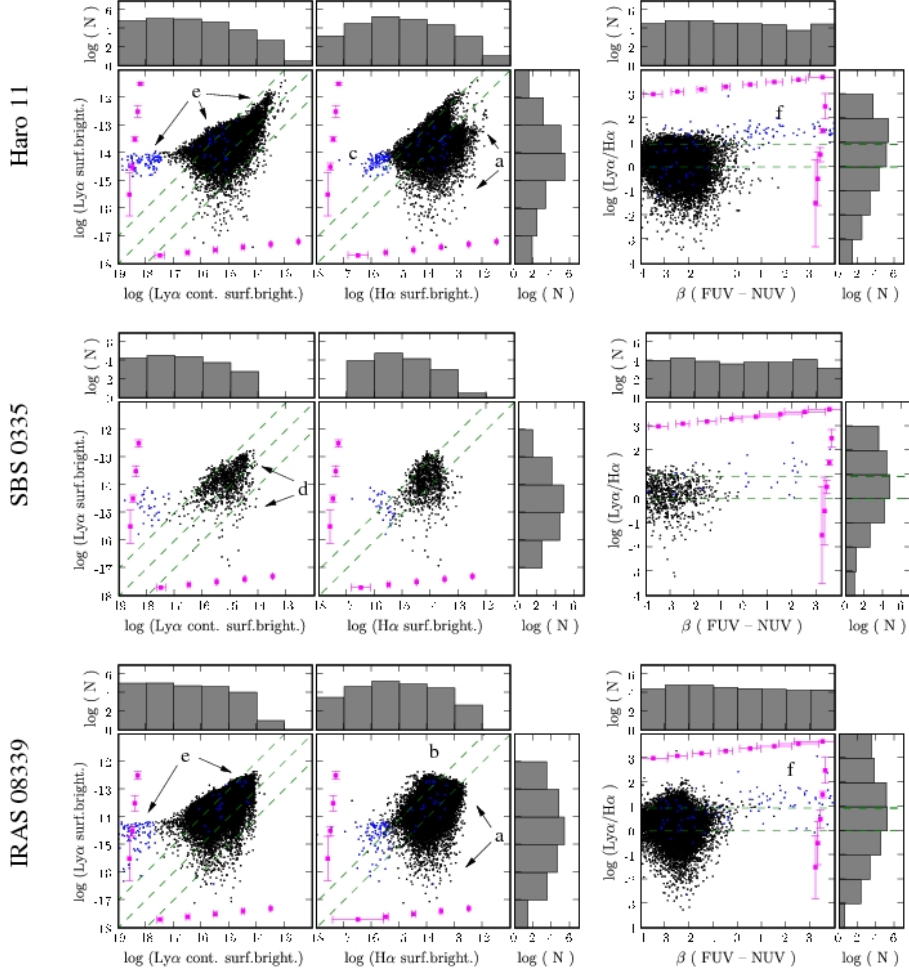


Fig. 4.— Pixel scatter distribution showing all ‘spaxels’ for which $S/N \geq 3$ in F140LP. Each spaxel, which may contain up to 1600 pixels of size $0.025''$ is represented by a single point. Black points show spaxels where $S/N \geq 10$ was attained, blue points show pixels in the range $3 < S/N < 10$. For the histograms, however, each spaxel is represented by the number of pixels that contributed to it, in order to show the true distribution. Since the ordinate shows the logarithm of the $\text{Ly}\alpha$ surface brightness, only spaxels with positive $\text{Ly}\alpha$ flux are included. Error-bars show the median statistical error in each magnitude bin for the ordinates and abscissae (placed diagonally to avoid overlap). *Left:* $\text{Ly}\alpha$ vs. UV surface brightness, here represented by the modeled continuum at 1216\AA , i.e. $\mu_{\lambda 1527} \times \text{CTN}$. The dashed lines show constant $\text{Ly}\alpha$ equivalent widths of 1, 10, and 100 \AA . *Center:* $\text{Ly}\alpha$ vs. $\text{H}\alpha$ surface brightness, both in units of $\text{erg/s/cm}^2/\text{arcsec}^2$. The dashed lines show $\text{Ly}\alpha = \text{H}\alpha$, and $\text{Ly}\alpha = 8.7\text{H}\alpha$ (Case B recombination). *Right:* $\text{Ly}\alpha/\text{H}\alpha$ line ratio vs. UV continuum slope β as derived from the fluxes in F140LP and F220M. *Top panels:* Haro 11. *Middle panels:* SBS 0335–052. *Bottom panels:* IRAS 08339+6517.

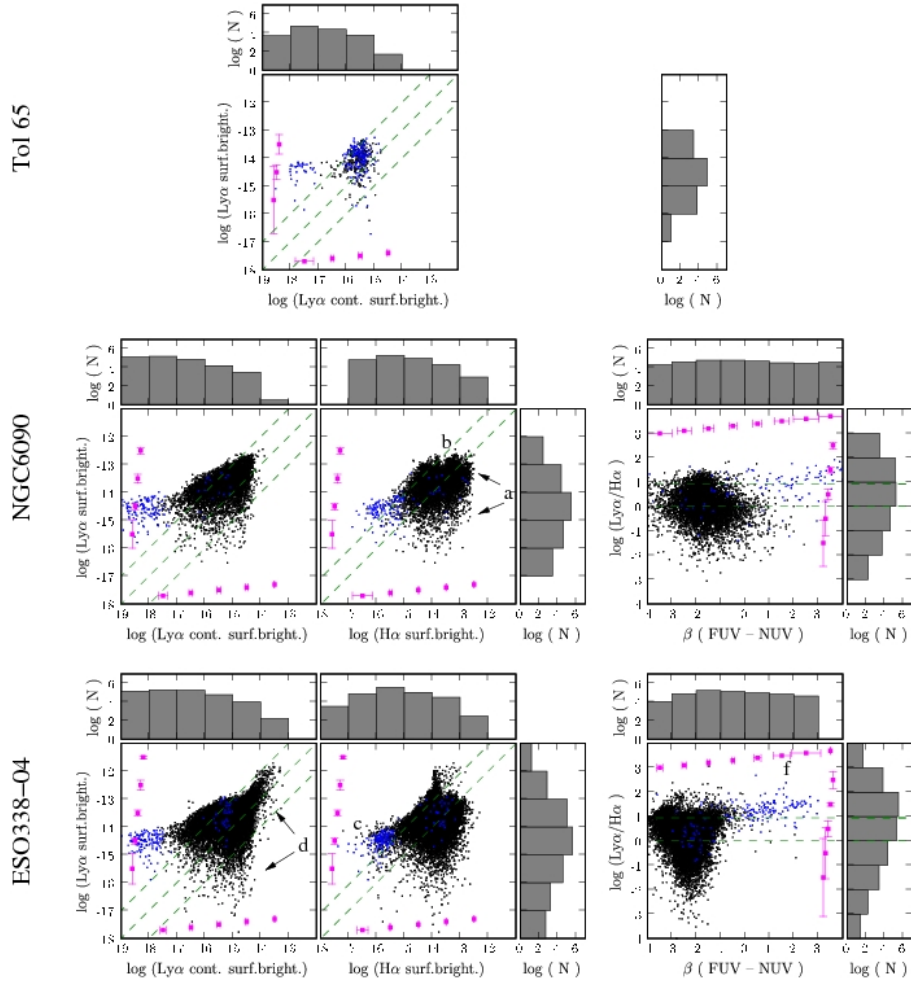


Fig. 5.— Same as Fig. 4 but for Tol 65 (top), NGC 6090 (middle) and ESO 338-04 (bottom). For Tol 65 we do not show $H\alpha$ since we only have reliable data at ground based resolution. For ESO 338-04 β was derived from the F140LP and F336W data. See caption of Fig. 4 for further details.

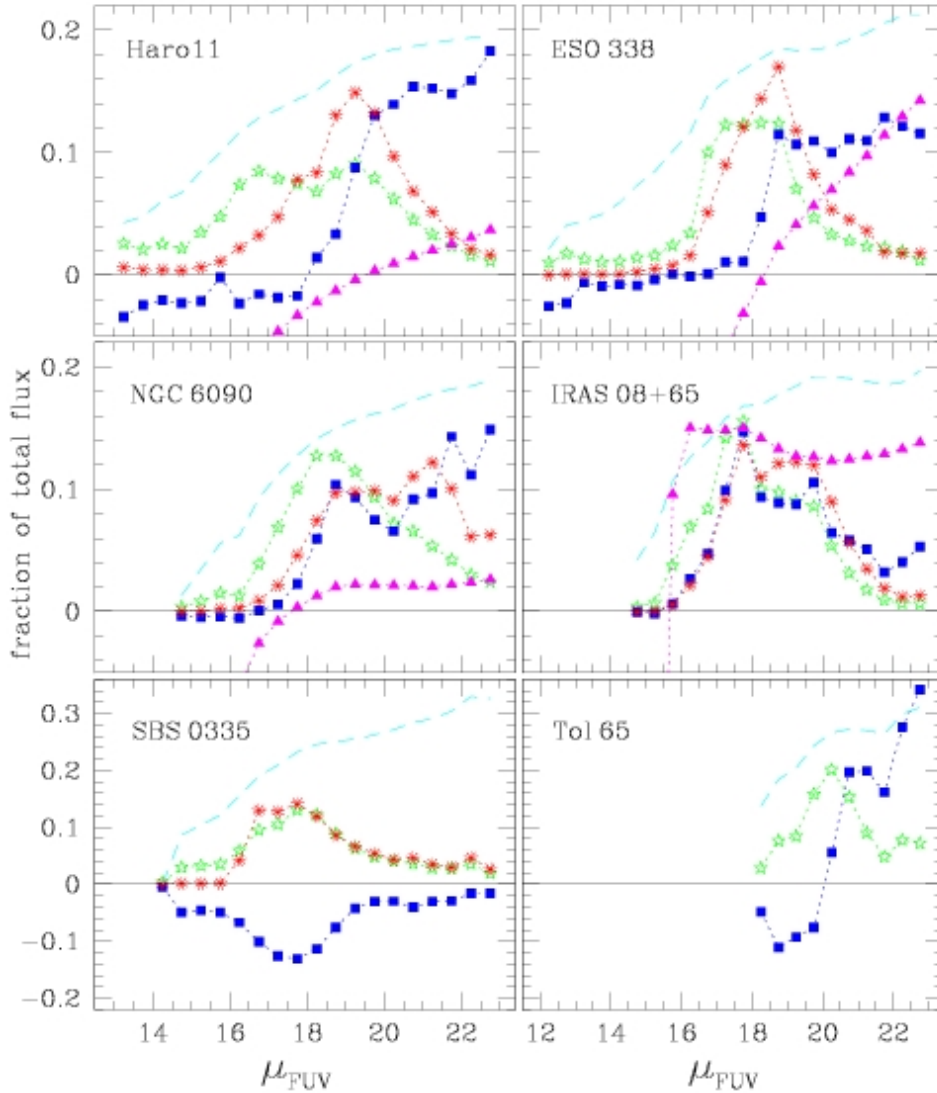


Fig. 6.— Flux distribution vs far UV surface brightness. Here we show the fraction of the total (within the $\mu_{AB,1500} = 23 \text{ mag}/\square''$ mask) flux as a function of $\mu_{AB,1500}$ (corrected for Galactic reddening only) summed in 0.5 magnitude bins. Stars (green) show 1500Å, filled squares (blue) show Ly α , and asterisks (red) show H α . Triangles (magenta) show the cumulative Ly α escape fraction, determined from H α – they always converge at the escape fraction presented in Table 5. Since the aperture mask is defined by making a surface brightness cut in F140LP, this demonstrates how the Ly α escape fraction may vary had this cut-off been chosen differently. The dashed lines (cyan) show $\log(N_{\text{pix}})/C$, the logarithm of the number of pixels in each 0.5 magnitude which, for the purpose of presentation, has been divided by a number C ($C = 22.5$ for all galaxies but SBS0335–052 and Tol65 where it is 12.5).

cape due to an outflowing neutral medium. In addition blueshifted metallic absorption lines indicated the presence of outflows along the line of sight. Bergvall et al. (2006) claimed a detection of Lyman continuum (LyC) photons escaping from this galaxy (but see also Grimes et al. 2007) and, since LyC does not scatter, porous ionized holes in the ISM are likely to exist along some sight-lines. The galaxy is very luminous in $H\alpha$ and has a high inferred star formation rate, still no HI or CO has been detected (Bergvall et al. 2003), the latter may be related to the low metallicity Bergvall & Östlin (2002).

This galaxy consists of three major star forming condensations although $Ly\alpha$ is seen directly in emission from only one (the NW knot; C in the nomenclature of Kunth et al. 2003). It is this knot that causes the high surface brightness features discussed in Section 4.4. The remaining two knots (one of which dominates the $H\alpha$ output) show $Ly\alpha$ absorption centered on the clusters themselves, with a patch of faint diffuse emission leaking from the condensation to the SW. The overall $Ly\alpha$ flux escaping is dominated by a diffuse component with $Ly\alpha/H\alpha$ ratios larger than the recombination value, indicating that most $Ly\alpha$ leaves the galaxy after multiple scatterings (see Hayes et al. (2007) for a description of the $Ly\alpha$ surface brightness profile). In the $Ly\alpha$ -bright eastern knot $Ly\alpha/H\alpha$ is close to the recombination value, and the EW is high, indicating that $Ly\alpha$ emission from this region may be avoiding resonant trapping and escaping more or less unhindered.

SBS 0335–052 Previous attempts have failed to detect anything but damped $Ly\alpha$ absorption from this galaxy (Thuan & Izotov 1997). Here we show, that while the central region is indeed characterized by $Ly\alpha$ absorption there are regions from which $Ly\alpha$ photons are emitted. Compared to the other galaxies, the fraction of $Ly\alpha$ emitting spaxels is small, but significant at the 3σ level. Integrated over the galaxy, it is a net absorber of $Ly\alpha$.

The brightest $Ly\alpha$ emitting spaxels have $Ly\alpha/H\alpha$ somewhat higher than the recombination value, which could result from resonant scattering, ISM geometry, or the production of additional $Ly\alpha$ photons by collisional excitation. This galaxy exhibits a low surface brightness tail just as the brighter $Ly\alpha$ emitters do.

The lack of a net positive escape at any surface brightness level is somewhat puzzling as the $Ly\alpha$ photons ought to get out somewhere, unless the density of static HI is so large that even moderate amounts of dust will destroy $Ly\alpha$.

IRAS 08339+6517 This is a spiral with a nuclear starburst. Kunth et al. (1998) found P-Cygni like emission, and Mas-Hesse et al. (2003) found further support for an ISM-kinematic regulation of the $Ly\alpha$ escape and evidence for recombinations in the outflowing shell. $Ly\alpha/H\alpha$ again supports a mixture of dust and kinematic effects in the ISM.

Since no F814W image was obtained for IRAS 08339+6517, our data-points are not sufficiently spread along the SED to fit two stellar populations, and continuum subtraction of $H\alpha$ also becomes less reliable. For IRAS 08339+6517 we therefore resort to a single component spectral fit using the standard stellar+nebular template from *Starburst 99*, i.e. method III in the terminology of Paper I.

Tol 65 This is the faintest galaxy in the sample, both in luminosity and apparent magnitude. In our HST $H\alpha$ image, the galaxy happened to fall outside the monochromatic patch of the ramp filter and could not be used. Hence, we had no information about the distribution of ionized gas at HST resolution and could not model the nebular emission as a separate component. Instead we used two stellar components where we used the option of *Starburst 99* to include the nebular continuum in the model (Leitherer et al. 1999). In addition, the ACS/SBC observations of Tol 65 suffered a guide star acquisition failure meaning that only one of the two guide stars were acquired, with the consequence that the telescope pointing could be drifting about the axis defined by the direction to the single guide star used. The images were registered manually rather than using MULTIDRIZZLE since the astrometric keywords could not be trusted. We have carefully examined the SBC images and found no evidence for a significant telescope drift during the observations, but the results for Tol 65 should be viewed with some caution.

To get a rough idea about the ionized gas distribution we retrieved a WFPC2 F555W image

of exposure time 1600s from the archive. The F555W and F550M filters have very similar central wavelength but, whereas F550M does not transmit any strong emission lines, F555W transmits $H\beta$, $[OIII]\lambda\lambda 4959, 5007$, and partly $H\alpha$. Thus, by subtracting F555W–F550M, scaled by their PHOT-FLAM values, we get a map of the strong emission lines, that can be used for qualitative purposes, e.g. in making the color image in Fig.3. For quantitative estimates of the $H\alpha$ flux and equivalent width, we have used ground-based data obtained from ESO’s New Technology Telescope (NTT) (Atek et al. 2008). Previous HST/GHRS spectra (Thuan & Izotov 1997) have indicated that the brightest knot is a damped $Ly\alpha$ absorber. The UV morphology of Tol65 is also rather complex but, assuming that the NW knot was acquired by the GHRS PEAK-UP maneuver, photometry performed in a $2'' \times 2''$ aperture consistently finds this to be an absorber.

Overall we find that the continuum-bright regions are dominated by absorption but we also see $Ly\alpha$ in emission from fainter regions. Tol65 is the galaxy for which the data quality is worst and the uncertainties are largest. Due to the effects discussed in Sect. 4.2, the positive net $Ly\alpha$ flux observed from this galaxy may not be real.

NGC 6090 This luminous starburst has a clear merger signature and is also very luminous in the IR. The star formation is concentrated to two regions both which show clear $Ly\alpha$ emission with emission/absorption varying on small scales. The $Ly\alpha/H\alpha$ ratio scatters between above the recombination value and absorption. The common tail of $Ly\alpha/H\alpha$ ratios is seen, extending to values that exceed the recombination value, and representing diffuse regions outside the star forming complexes.

ESO 338–04 The $Ly\alpha$ morphology of this galaxy was discussed in Hayes et al. (2005) using a less sophisticated method (similar to method III in the terminology of Paper I) for continuum subtraction which was based on a single stellar population and did not include a separate treatment of the nebular continuum. Our new results are, however, in good agreement with Hayes et al. (2005). The starburst is dominated by a rich population of young massive star clusters (Östlin et al. 1998, 2003), around which strong $H\alpha$ is seen following a

rich and detailed structure consisting of shells and filaments. In contrast the $Ly\alpha$ emission is much more extended and clearly asymmetric with the main emission in the N–S direction, where there are signs of outflows from other investigations (e.g. Östlin et al. 2001, 2007). Central patches of $Ly\alpha$ absorption are seen across much of the central star forming complex with a noticeable streak in the E–W direction. This is not seen in age or $E(B-V)$ maps and is most likely the result of a filamentary HI structure lying in front of the starburst. Unique for this galaxy is the clear vertical tail to super recombination values in the $Ly\alpha vs H\alpha$ distribution occurring also at bright levels (Knot A in the nomenclature of Hayes et al. (2005). See Fig. 5).

5. Discussion

All targets reveal $Ly\alpha$ morphologies qualitatively very different from those revealed by the FUV continuum or $H\alpha$. Two $Ly\alpha$ non-emitters (SBS 0335–052 and Tol65) were on purpose included in the sample, but both show signatures of $Ly\alpha$ leakage, and one of them is actually found to be a net $Ly\alpha$ emitter (Tol65), although this is our object with the poorest data quality. In the remaining cases (Haro 11, IRAS 08339+6517, NGC 6090, ESO 338–04) where the $Ly\alpha$ signature is very clear and well-structured, the equivalent widths are found to be low with line-ratios significantly lower than the recombination value, and escape fractions well below unity.

Our targets span luminosities from the dwarf regime to that of $z \sim 0.15$ compact UV-luminous galaxies (UVLGs) that have been proposed as local analogs of LBGs by virtue of their luminosity and morphology (Overzier et al. 2008). Indeed, Haro 11 was used in their paper as a local comparison object. Although their selection did not favour inclusion of galaxies with multiple nuclei, such as Haro 11 or NGC 6090 our four most luminous galaxies otherwise have very similar properties to UVLGs. Morphologically, and in terms of rest rest-frame colors and luminosities our sample galaxies are also similar to starbursts at $z \sim 1$ studied in deep HST U-band images (de Mello et al. 2006).

5.1. Emission scales and porosity

In front of the star forming regions we find strong variations in both the Ly α images and equivalent width maps, ranging between absorption and emission. This phenomenon is seen on scales ranging between the smallest we can probe reliably (0.1'', corresponding to a physical sizes ranging between 20 and 60 pc) up to sizes an order of magnitude larger. The scatter plots (Figs. 4 and 5) clearly show the large variation of Ly α equivalent width (for positive spaxels) from the regions of peak UV and H α surface brightness. There is no apparent characteristic size over which these variations are seen. That is, the Ly α flux or $W_{\text{Ly}\alpha}$ may be radically different, e.g. switching from absorption to emission, even on the smallest scales we can probe. This supports the model in which Ly α may escape through favorable paths in a porous and inhomogeneous ISM. However, it is also clear that this is not the main mechanism by which Ly α photons escape galaxies, because the net emission, if any, is always dominated by diffuse emission from regions with low UV and Ly α surface brightness.

In Figure 6 we have presented the fractional contribution to the total Ly α and H α emission as a function of UV surface brightness. Four out of five targets (Tol 65 was not observed in H α) show a systematic offset between H α and FUV (red lines appear shifted towards fainter levels compared to green), which can be expected for two reasons: Firstly, the ionization boundary will be extended away from clusters, where UV surface brightness is lower and may be resolved in the images. Secondly, stellar mechanical feedback may blow out the ionized ISM in shells and filaments, further decoupling the nebular and stellar components. Likely this is true also for Tol 65 since, like in the other four cases, Ly α is offset with respect to FUV. Ly α is in general further (compared to H α) offset towards lower FUV surface brightness levels, demonstrating the importance of additional scatterings affecting Ly α .

The only object that does not show a systematic offset between FUV and H α surface brightness is SBS 0335–052. Mas-Hesse et al. (2003) suggested that damped Ly α absorption profile observed in this galaxy to be due to the youth of the starburst episode ($W_{\text{H}\alpha} = 1500\text{\AA}$); insufficient

time has elapsed to generate a strong wind and accelerate the surrounding H I. The fact that we observe H α and FUV emission from SBS 0335–052 to be rather tightly correlated could also be a reflection of this fact, and is consistent with the interpretation. The Ly α line, on the other hand, almost completely mirrors that of the FUV, and is seen only in strong absorption in the central regions. This is naturally an effect of absorption of the stellar continuum as discussed in Section 4.2, where more flux appears to be absorbed at higher surface brightness.

IRAS 08339+6517 and, to a lesser degree, NGC 6090 shows some degree of correlation between the relative H α emission and Ly α . However, at intermediate UV surface brightness ($\mu_{\text{AB},1500} = 18$ to 20 mag/''²) systematically less Ly α is emerging with respect to H α than at fainter continuum levels. Again this is indicative of the resonant scattering of Ly α increasing typical physical scales of the emission and resulting in low-level emission outside the starburst region.

The remaining strongly emitting galaxies, Haro 11, and ESO 338–04 show strong and systematic offsets between the surface brightnesses where the bulk of the H α and Ly α emerge. This is nicely illustrated also in Figures 1, 2, and 3 where large scale Ly α emission is seen from outside the star forming regions. In Haro 11, the peak in the output Ly α luminosity distribution is offset from H α by about 2.5 magnitudes in $\mu_{\text{AB},1500}$. In ESO 338–04 the bulk of the Ly α output is shown clearly to be at faint UV flux levels although no clear maximum is seen and much Ly α emerges from the faintest UV bin.

Clear signatures of diffuse Ly α emission, above the level of the background residuals is seen in both Haro 11 and ESO 338–04 at radial distances from the central star-forming region of around 3 and 1.5 kpc, respectively.

5.2. Ly α escape fraction and dust

Unlike non-resonant radiation, photon scattering causes Ly α to be emitted over larger areas than radiation in the adjacent continuum and at lower local signal-to-noise where it is more susceptible to contamination by residuals from the sky-background and flatfielding. Thus the measured Ly α escape fraction may be a strong func-

tion of aperture which is evident from Fig 6. Had our data been deeper and we could have been more confident about photometry at very faint levels, the escape fractions may well have increased. For a case like SBS 0335–052, which is not very dusty, one would naively expect most of the Ly α to emerge somewhere – indeed a significant fraction of H α emission comes from outside our aperture mask. On the other hand, when we fit a Sérsic profile to the Ly α scattering component of Haro 11 at good S/N (Hayes et al. 2007) and integrated the flux to an infinite radius, we obtained a flux consistent with aperture photometry within a few per-cent. For reference, to reach S/N=10 in a 1 \square '' aperture, a source of the same surface brightness as the average spaxel-to-spaxel sky variation (see Table 4) would require over 30 orbits in SHADOW mode with SBC/F122M per target.

Five out of six cases are found to be net Ly α emitters with Ly α escape fractions in the range 3 to 14 percent. From the sixth galaxy (SBS 0335–052), we do detect some Ly α emission leaking outside the central starburst region. However, also at faint levels is the net integrated Ly α flux negative. It is possible that more Ly α would have been detected in the case that our observations would have been deeper, allowing us to probe greater radii. This of course applies to all our galaxies: the regions for which the Ly α and H α fluxes have been integrated is significantly smaller than the total optical extent of the galaxies and we may be missing a non-negligible fraction of the diffuse emission. The Ly α escape fractions should in this respect be seen as lower limits. On the other hand, some galaxies may contain star forming regions that are so dusty that not even any H α escapes in which case the actual Ly α escape fractions would be lower.

Our modeling software provides us with an estimate of the reddening of the stellar continuum below Ly α ; this is what is required for the subtraction of the continuum from the F122M filter. However, due to geometrical differences in the configuration of stars and nebular gas, stellar and nebular $E(B-V)$ measurements are shown to differ (Maiz-Apellaniz et al. 1998; Mas-Hesse & Kunth 1999; Charlot & Fall 2000; Calzetti et al. 2000). Thus we have little information about the reddening in the gas in which Ly α is formed. While differences in the respective reddening measurements can be

expected to minimize with increasing spatial resolution of the observation, geometrical differences between the stellar and nebular components along the line-of-sight will always be present. Firstly, we know that Ly α and Balmer lines must be produced in the same ionized nebulae. Secondly, we may suspect that due to resonant scattering increasing the traversed path-length, Ly α photons should experience at least the reddening of the Balmer lines, although certain geometrical configurations may be envisaged that make this statement uncertain. Evidently, some circumspection must be exercised when comparing derived reddening with the emission (or absorption) of Ly α . With this cautionary remark in mind, we deem it interesting to de-redden the Ly α fluxes (using the reddening found from the SED fit), recompute the Ly α escape fractions, and explore to what extent pure dust attenuation can be said to regulate the fraction of escaping Ly α photons. In that case we would expect to find $\mathcal{R} = 1$. After de-reddening we find \mathcal{R} values between 13% (NGC 6090) and 40% (ESO 338–04). Hence, even in our dustiest case (NGC 6090) the observed stellar reddening is insufficient in explaining the attenuation of Ly α .

Figure 7 shows where the galaxies fall when $f_{esc, Ly\alpha}$ and \mathcal{R} are compared with $E(B-V)$. Any correlation present for such a small sample must be viewed upon with skepticism, but the emitters with lowest $E(B-V)$ do have higher escape fractions. ESO 338–04 is a dust-poor galaxy with the integrated measurement from this study finding $E(B-V) = 0.076$. Nevertheless, the applied dust correction does play a significant role, with the same conclusion being reached for IRAS 08339+6517, and also perhaps for Haro 11. \mathcal{R} in some sense can be thought of as a measure of the importance of resonant scattering but the effect is so non-linear that quantification is not possible.

To strengthen the analysis performed here we would need to independently map the nebular extinction, at least mitigating the potential difficulties that arise from blended stars and gas. Such a study is performed at $\sim 1''$ resolution in (Atek et al. 2008) and we are currently exploring the use of adaptive optics imaging in the Br γ line for two galaxies.

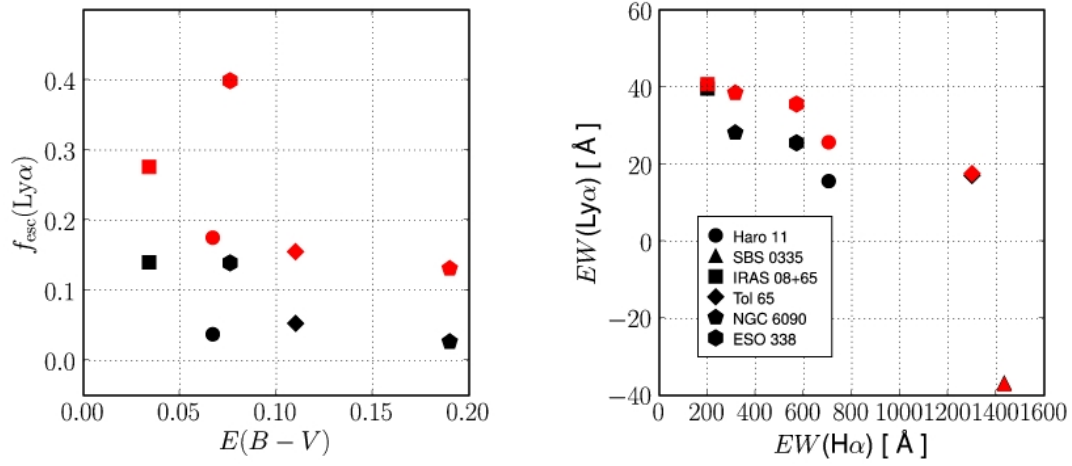


Fig. 7.— Scatter plots for the complete sample: Haro 11 (circle); SBS 0335–052 (triangle); IRAS 08339+6517 (square); Tol 65 (diamond); NGC 6090 (pentagon); ESO 338–04 (hexagon). *Left*: $\text{Ly}\alpha$ escape fraction reddening *vs.* $E(B-V)$. Black points show the observed escape fractions, and red the escape fractions corrected for internal extinction. Since SBS 0335–052 is a net absorber, it is not shown. *Right*: $W_{\text{Ly}\alpha}$ *vs.* $W_{\text{H}\alpha}$. Again, black points show the observed values, while for red symbols $\text{Ly}\alpha$ and $\text{H}\alpha$ have been corrected for the fitted $E(B-V)$.

5.3. Equivalent widths

Comparing $W_{\text{Ly}\alpha}$ or the $\text{Ly}\alpha$ escape fractions with most of the parameters listed in Table 5 yields almost nothing in the way of trends. Indeed this study has never aimed to provide any statistical answers and with only a sample of six objects could hardly be considered statistically meaningful. Moreover, since the sample was designed to sample a range of starburst parameters and include emitters and non-emitters of $\text{Ly}\alpha$, any trends may purely be a feature of the selection. That said, the anti-correlation of $W_{\text{Ly}\alpha}$ and $W_{\text{H}\alpha}$ mentioned in Section 4.3 is indeed interesting as it seems to be rather tight, although this trend is not seen in the $\text{Ly}\alpha$ escape fraction, with or without dust correction. From the *Starburst 99* models, we estimate that our lowest globally measured $W_{\text{H}\alpha}$ corresponds to an age of around 6 Myr for an instantaneous burst, solar metallicity and Salpeter IMF. Higher $W_{\text{H}\alpha}$ naturally corresponds to younger ages, with equivalent widths of several thousand Å expected during the first 3 Myr or so. In the studies of Tenorio-Tagle et al. (1999) and Mas-Hesse et al. (2003) it is concluded that at the youngest times, $\text{Ly}\alpha$ may be expected in absorption, followed by an emission phase when the mechanical energy return from star formation has accelerated the ambient medium. How the expected equivalent widths of $\text{Ly}\alpha$ and $\text{H}\alpha$ co-evolve is difficult to predict, and instantaneous burst assumption is certainly an oversimplification when dealing with global properties. Nevertheless, what we are seeing may be a direct consequence of evolution.

Related to the $\text{Ly}\alpha$ escape fraction and equivalent width is the escape fraction of Lyman continuum (i.e. ionizing) photons. Some Lyman continuum must escape from galaxies at very high- z in order to explain the reionization of the universe which apparently was complete by $z \sim 6$ (Fan et al. 2006).

Escaping Lyman continuum photons would not contribute to photoionization within galaxies and would thus lower the luminosities and equivalent widths of $\text{Ly}\alpha$ and other Hydrogen recombination lines. However, Lyman continuum leakage would not necessarily lower the $\text{Ly}\alpha$ escape fractions or the $\text{Ly}\alpha/\text{H}\alpha$ ratios. On the contrary, the existence of HI clear paths through the ISM would also pro-

mote $\text{Ly}\alpha$ escape.

Oey et al. (2007) studied the ISM in nearby galaxies and their result suggest that in starbursts, i.e. galaxies with high $\text{H}\alpha$ surface brightness, some of the Lyman continuum radiation might be leaking out, and there is tentative direct detection of Lyman continuum emission in Haro 11 (see Sect. 4.5). At high redshift, determining direct escape fractions really means pushing the observational capabilities, and implied escape fractions are in general low (Siana et al. 2007), although several galaxies have been found with significant Lyman continuum leakage (Shapley et al. 2006).

6. Perspectives

Not only is $\text{Ly}\alpha$ currently the most favorable window on the galaxy population at high- z but it is expected to remain so. Balmer lines are naturally much easier to interpret than $\text{Ly}\alpha$ but their longer rest-wavelength makes them less suitable for high- z . The James Webb Space Telescope promises huge improvements, particularly regarding $\text{H}\alpha$ imaging and spectroscopy at high- z and near- and mid-IR continuum observations from an environment free from atmospheric background emission. However, at $z \gtrsim 6$, $\text{H}\alpha$ will be redshifted out of the bandpasses of NIRCAM and NIRSPEC, leaving only MIRI with limited field-of-view and multiplexing capabilities for the detection of $\text{H}\alpha$. Thus especially if $\text{Ly}\alpha$ is, as predicted, visible from beyond the epoch of reionization (e.g. Cen & Haiman 2000) then $\text{Ly}\alpha$ is likely to remain one of the primary probes of the high redshift universe for the coming decades.

Some rather interesting possible trends have been identified and to improve on the study presented here a number of alternatives can be envisaged. Comparison of the co-evolution of $W_{\text{Ly}\alpha}$ and $W_{\text{H}\alpha}$ yields results that are difficult to attach meaning to in a small, hand-picked sample. What is required to rectify this is an imaging survey of nearby star-forming galaxies in $\text{Ly}\alpha$, selected in a clean homogeneous manner. Some of the targets presented here are of sufficient star-formation rate and FUV luminosity that they may be directly comparable to some of the objects being studied by high- z $\text{Ly}\alpha$ observations and such a low- z sample would prove extremely valuable for co-interpretation of the survey data. Indeed, sim-

ulations for such a study have already been performed (Paper I) and have demonstrated that results of similar reliability to those presented here may be obtained with a slightly reduced number of filters.

The use of HST for this project was initially motivated by the need for a FUV-capable space-based imager to observe Ly α at $z \sim 0$ and not primarily driven by the high spatial resolution. Given that we see variations in Ly α between emission and absorption on scales down to the resolution limit of the telescope, the need for the high resolving power has become essential. H β obtained with HST would permit a direct examination of extinction in the gas phase, an analysis of the role of dust on a pixel-by-pixel basis, a better evaluation of the ionizing photon production, and would also enable us to lock the nebular $E(B - V)$ in the continuum fitting software. An alternative that we are currently exploring is the use of ground-based adaptive optics NIR imaging in the Br γ line using the NAOS-CONICA instrument on ESO's VLT.

7. Conclusions

We have produced continuum subtracted and calibrated Ly α and H α images for a sample of six local star-forming galaxies using the Advanced Camera for Surveys onboard Hubble Space Telescope. Morphological and photometric analyses have been performed on the Ly α , H α and stellar continuum maps. In summary:

- A variety of morphologies is found, ranging from general absorption to emission. Absorption and emission in individual targets are found to change on scales down to the resolution limit of the telescope. Ly α features in emission and absorption show only minor correlation with the stellar morphology.
- Typically Ly α emission is seen on large scales surrounding the central star forming regions in the form of low surface brightness halos. Moreover, Ly α is found to be more spatially extended than H α and appears to emerge almost preferentially at low FUV surface brightnesses. At fainter isophotal levels, Ly α is typically seen in emission, with fluxes and equivalent widths greater

than those that would be predicted from recombination theory.

- Observed Ly α escape fractions range from below 0 (absorber) to about 14%. Normal corrections for internal dust extinction are insufficient to explain these values.
- Although any trends found from such a small hand picked sample must be viewed with caution, the found anti-correlation between the equivalent widths of Ly α and H α is quite suggestive. This could be explained if Ly α escape is regulated by feedback, i.e. the development of wind blown bubbles and ISM flows that allow the photons to avoid the resonant trapping by static H I.
- All the above statements point directly to one conclusion: the phenomenon of resonant scattering is observed to be extremely important in the regulation of Ly α emission, and radiative transfer of Ly α photons in star-forming galaxies.
- A few of our galaxies have far ultraviolet luminosities comparable to some of the objects being studied through their Ly α emission at the highest redshifts. Given the low Ly α escape fractions and complex resonant scattering phenomenon under observation here, care should be executed in interpretation of high- z survey data.
- Our sample is fully calibrated and of physical resolution three orders of magnitude better than the observed candidates at high- z . It may therefore be valuable in interpretation of high- z datasets and of use to compare with the output of radiative transfer codes. The images are being released to the community.

As a service to the community we release calibrated Ly α , H α , and their respective continuum images to the public domain, for the purpose of modeling high- z galaxies and Ly α radiative transfer. The images and documentation are available at *Centre de Données astronomiques de Strasbourg (CDS)* and also at the following website: <http://ttt.astro.su.se/projects/Lyman-alpha/>

Other data products, such as maps of age and reddening and Lyman continuum production will be available upon request.

GÖ and MH acknowledge the support from the Swedish National Space Board (SNSB) and the Research Council (Vetenskapsrådet). We thank D. Schaerer for useful discussions.

REFERENCES

- Adams, T. F. 1972, *ApJ*, 174, 439
- Ahn, S.-H. 2004, *ApJ*, 601, L25
- Ajiki, M., Taniguchi, Y., Fujita, S. S., et al. 2003, *AJ*, 126, 2091
- Atek, H., Kunth, D., Hayes, M., Östlin, G., & Mas-Hesse, J. M. 2008, *A&A*
- Bergvall, N., Laurikainen, E., & Aalto, S. 2003, *A&A*, 405, 31
- Bergvall, N. & Östlin, G. 2002, *A&A*, 390, 891
- Bergvall, N., Zackrisson, E., Andersson, B.-G., et al. 2006, *A&A*, 448, 513
- Bremer, M. N., Lehnert, M. D., Waddington, I., et al. 2004, *MNRAS*, 347, L7
- Brocklehurst, M. 1971, *MNRAS*, 153, 471
- Calzetti, D., Armus, L., Bohlin, R. C., et al. 2000, *ApJ*, 533, 682
- Calzetti, D. & Kinney, A. L. 1992, *ApJ*, 399, L39
- Cappellari, M. & Copin, Y. 2003, *MNRAS*, 342, 345
- Cen, R. & Haiman, Z. 2000, *ApJ*, 542, L75
- Charlot, S. & Fall, S. M. 1993, *ApJ*, 415, 580
- . 2000, *ApJ*, 539, 718
- Cowie, L. L. & Hu, E. M. 1998, *AJ*, 115, 1319
- de Mello, D. F., Wadadekar, Y., Dahlen, T., Casertano, S., & Gardner, J. P. 2006, *AJ*, 131, 216
- Diehl, S. & Statler, T. S. 2006, *MNRAS*, 368, 497
- Dijkstra, M., Wyithe, J. S. B., & Haiman, Z. 2007, *MNRAS*, 379, 253
- Fujita, S. S., Ajiki, M., Shioya, Y., et al. 2003, *AJ*, 125, 13
- Giallisco, M., Koratkar, A., & Calzetti, D. 1996, *ApJ*, 466, 831
- Gonzalez Delgado, R. M., Leitherer, C., Heckman, T., et al. 1998, *ApJ*, 495, 698
- Gronwall, C., Ciardullo, R., Hickey, T., et al. 2007, *ArXiv e-prints*, 705
- Hansen, M. & Oh, S. P. 2006, *MNRAS*, 367, 979
- Harrington, J. P. 1974, *MNRAS*, 166, 373
- Hayes, M. & Östlin, G. 2006, *A&A*, 460, 681
- Hayes, M., Östlin, G., Atek, H., et al. 2007, *MNRAS*, 382, 1465
- Hayes, M., Östlin, G., Mas-Hesse, J. M., & Kunth, D. 2008, *AJ*
- Hayes, M., Östlin, G., Mas-Hesse, J. M., et al. 2005, *A&A*, 438, 71
- Hu, E. M., Cowie, L. L., Capak, P., et al. 2004, *AJ*, 127, 563
- Iwata, I., Ohta, K., Tamura, N., et al. 2003, *PASJ*, 55, 415
- Izotov, Y. I., Chaffee, F. H., & Green, R. F. 2001, *ApJ*, 562, 727
- Kashikawa, N., Shimasaku, K., Malkan, M. A., et al. 2006, *ApJ*, 648, 7
- Kodaira, K., Taniguchi, Y., Kashikawa, N., et al. 2003, *PASJ*, 55, L17
- Kudritzki, R.-P., Méndez, R. H., Feldmeier, J. J., et al. 2000, *ApJ*, 536, 19
- Kunth, D., Leitherer, C., Mas-Hesse, J. M., Östlin, G., & Petrosian, A. 2003, *ApJ*, 597, 263
- Kunth, D., Lequeux, J., Sargent, W. L. W., & Viallefond, F. 1994, *A&A*, 282, 709
- Kunth, D., Mas-Hesse, J. M., Terlevich, E., et al. 1998, *A&A*, 334, 11
- Law, D. R., Steidel, C. C., Erb, D. K., et al. 2007, *ApJ*, 656, 1

- Le Delliou, M., Lacey, C., Baugh, C. M., et al. 2005, *MNRAS*, 357, L11
- Leitherer, C., Schaerer, D., Goldader, J. D., et al. 1999, *ApJS*, 123, 3
- Lequeux, J., Kunth, D., Mas-Hesse, J. M., & Sargent, W. L. W. 1995, *A&A*, 301, 18
- Lotz, J. M., Madau, P., Giavalisco, M., Primack, J., & Ferguson, H. C. 2006, *ApJ*, 636, 592
- Maiz-Apellaniz, J., Mas-Hesse, J. M., Munoz-Tunon, C., Vilchez, J. M., & Castaneda, H. O. 1998, *A&A*, 329, 409
- Malhotra, S. & Rhoads, J. E. 2002, *ApJ*, 565, L71
- Mas-Hesse, J. M. & Kunth, D. 1999, *A&A*, 349, 765
- Mas-Hesse, J. M., Kunth, D., Tenorio-Tagle, G., et al. 2003, *ApJ*, 598, 858
- Meier, D. L. 1976, *ApJ*, 207, 343
- Meier, D. L. & Terlevich, R. 1981, *ApJ*, 246, L109
- Neufeld, D. A. 1990, *ApJ*, 350, 216
- . 1991, *ApJ*, 370, L85
- Nilsson, K. K., Moeller, P., Moeller, O., et al. 2007, *ArXiv e-prints*, 706
- Oey, M. S., Meurer, G. R., Yelda, S., et al. 2007, *ApJ*, 661, 801
- Osterbrock, D. E. 1962, *ApJ*, 135, 195
- Östlin, G., Amram, P., Bergvall, N., et al. 2001, *A&A*, 374, 800
- Östlin, G., Bergvall, N., & Roennback, J. 1998, *A&A*, 335, 85
- Östlin, G., Cumming, R. J., & Bergvall, N. 2007, *A&A*, 461, 471
- Östlin, G., Zackrisson, E., Bergvall, N., & Rönnback, J. 2003, *A&A*, 408, 887
- Ouchi, M., Shimasaku, K., Akiyama, M., et al. 2005, *ApJ*, 620, L1
- Ouchi, M., Shimasaku, K., Furusawa, H., et al. 2003, *ApJ*, 582, 60
- Overzier, R. A., Heckman, T. M., Kauffmann, G., et al. 2008, *ApJ*, 677, 37
- Papaderos, P., Izotov, Y. I., Guseva, N. G., Thuan, T. X., & Fricke, K. J. 2006, *A&A*, 454, 119
- Partridge, R. B. & Peebles, P. J. E. 1967, *ApJ*, 147, 868
- Prévot, M. L., Lequeux, J., Prevot, L., Maurice, E., & Rocca-Volmerange, B. 1984, *A&A*, 132, 389
- Ravindranath, S., Giavalisco, M., Ferguson, H. C., et al. 2006, *ApJ*, 652, 963
- Rhoads, J. E., Dey, A., Malhotra, S., et al. 2003, *AJ*, 125, 1006
- Rhoads, J. E. & Malhotra, S. 2001, *ApJ*, 563, L5
- Salpeter, E. E. 1955, *ApJ*, 121, 161
- Schaerer, D. 2003, *A&A*, 397, 527
- Schlegel, D. J., Finkbeiner, D. P., & Davis, M. 1998, *ApJ*, 500, 525
- Shapley, A. E., Steidel, C. C., Pettini, M., & Adelberger, K. L. 2003, *ApJ*, 588, 65
- Shapley, A. E., Steidel, C. C., Pettini, M., Adelberger, K. L., & Erb, D. K. 2006, *ArXiv Astrophysics e-prints*
- Shimasaku, K., Kashikawa, N., Doi, M., et al. 2006, *PASJ*, 58, 313
- Shimasaku, K., Ouchi, M., Furusawa, H., et al. 2005, *PASJ*, 57, 447
- Siana, B., Teplitz, H. I., Colbert, J., et al. 2007, *ApJ*, 668, 62
- Stanway, E. R., Bunker, A. J., & McMahon, R. G. 2003, *MNRAS*, 342, 439
- Sunyaev, R. A., Tinsley, B. M., & Meier, D. L. 1978, *Comments on Astrophysics*, 7, 183
- Taniguchi, Y., Ajiki, M., Nagao, T., et al. 2005, *PASJ*, 57, 165
- Tenorio-Tagle, G., Silich, S. A., Kunth, D., Terlevich, E., & Terlevich, R. 1999, *MNRAS*, 309, 332

- Thuan, T. X. & Izotov, Y. I. 1997, ApJ, 489, 623
- Venemans, B. P., Röttgering, H. J. A., Overzier, R. A., et al. 2004, A&A, 424, L17
- Verhamme, A., Schaerer, D., & Maselli, A. 2006, A&A, 460, 397
- Windhorst, R. A., Taylor, V. A., Jansen, R. A., et al. 2002, ApJS, 143, 113